Multi-quanta energy relaxation in a nonlinear quantum dimer coupled to a phonon bath

Vincent J.C. Pouthier

Multi-quanta energy relaxation in a nonlinear quantum dimer coupled to a phonon bath

Vincent Pouthier

Université de Franche Comté, UMR CNRS 6624, Laboratoire de Physique Moléculaire, 25030 Besançon cedex - France

Abstract

A quantum kinetic equation is established for describing the vibrational dynamics of a nonlinear quantum dimer coupled to a phonon bath. It is shown that a critical value of the number of quanta discriminates between two dynamical regimes for the population difference of quanta between the two sites of the dimer. Below the critical value, the population difference shows low-frequency damped oscillations revealing a coherent energy transfer associated to the delocalization of a V-quanta bound state. Nevertheless, these oscillations decay due to the coupling with the phonon bath so that the dimer reaches an equilibrium configuration in which the population is uniformly distributed over the two sites. In addition, its exponential decay supports a small amplitude high frequency modulation in the short time limit. Above the critical value, the population difference is almost constant in the short time limit although it still supports a small amplitude high-frequency modulation. Then, in the long time limit, the coherent energy transfer has disappeared and the population difference exhibits a purely incoherent exponential decay to finally converge to the equilibrium.

Key words: Nonlinear quantum dimer; Vibrons; Polarons; Bound states; Quantum breathers; Relaxation

1 Introduction

Although the energy released by the hydrolysis of adenosine triphophate (ATP) is a universal source allowing many biological processes, the fundamental question arises whether it can be transported from the active sites of a cell to other regions without being dispersed or dissipated. This feature was first pointed out by Davydov and co-workers to explain the vibrational energy flow in α-helices [1]. The main idea is that the released energy, stored in the high-frequency amide-I vibration of a peptide group, delocalizes along the helix

leading to the formation of vibrational excitons called vibrons. Their interaction with the phonons of the helix induces a nonlinear dynamics which counterbalances the dispersion. It yields the creation of the so called Davydov's soliton which is the solution of the Nonlinear Schrodinger (NLS) equation within the continuum approximation [2,3]. Moreover, the discrete version of NLS yields the occurrence of discrete breathers which correspond to time-periodic and spatially localized solutions [4–6]. Contrary to solitons, they do not require integrability for their existence and stability and they correspond to quite general and robust solutions [7].

Unfortunately, no clear evidence has yet been found for the existence of these nonlinear objects in real proteins and it has been suggested that the solution is rather a small polaron than a soliton [8–12]. Indeed, the vibron bandwidth in proteins is smaller than the phonon cutoff frequency. Therefore, the non-adiabatic limit is reached and the quantum behavior of the phonons is fundamental. A vibron is thus dressed by a virtual cloud of phonons which yields a lattice distortion essentially located on a single site and which follows instantaneously the vibron. The dressed vibron forms the small polaron.

Recently, the polaron approach has been improved to include the anharmonicity of each amide-I mode [13–17]. When two quanta are excited, the intramolecular anharmonicity and the dressing effect favor an attractive interaction between them leading to the occurrence of two-polaron bound states (TPBS). A bound state corresponds to the trapping of the two quanta over only a few neighboring sites with a resulting energy which is lesser than the energy of two quanta lying far apart. The separating distance between the two quanta is localized so that they behave as a single particle delocalized along the lattice with a well-defined momentum. Since TPBS are the first quantum states which experience the nonlinearity, they can be viewed as the quantum counterpart of breathers or solitons [13,14,18–28]. Note that a recent experiment devoted to the femtosecond infrared pump-probe spectroscopy of the N-H mode in a stable α-helix [29] was successfully interpreted within this approach.

Within the polaron formalism, the strong vibron-phonon interaction is partially removed so that a polaron-phonon coupling remains. This coupling, assumed to be small enough to be treated using standard perturbation theory, has been disregarded in most of the previous works. Therefore, the aim of this paper is to address a comprehensive theory to describe the influence of this coupling onto the dynamics of bound states involving a large number of polarons. For that purpose, we consider a simple system formed by two nearest neighbor amide-I modes embedded in an extended perfect lattice, i.e. a nonlinear quantum dimer coupled to a phonon bath.

Within the semi-classical approximation, the dimer is described by two coupled NLS equations which give rise to a transition between a delocalized and a

self-trapped dynamics [30]. Kenkre and Campbell [31] demonstrated the transition by using a closed nonlinear equation for the site-occupation probability difference in terms of Jacobian elliptic functions. Then, this model was extended to include dissipation effects [32–34], asymmetry [35–39], and several other aspects [40–45]. By contrast, the self-trapping transition does not occur in the quantum regime since the eigenstates of the dimer share the symmetry of the reflection operator which commutes with the dimer Hamiltonian [46,47]. As a consequence, they cannot localize the energy. Nevertheless, both the nonlinearity and the number of quanta control the timescale in the course of which the energy is exchanged coherently between the two sites. When several quanta are initially localized on a given site, the population difference between the two sites exhibits a rich behavior on different timescales ranging from small amplitude oscillations and collapses and revivals, to coherent tunneling [48–50].

At present, because the nature of a quantum nonlinear dimer is relatively well understood, we investigate the influence of a coupling with a phonon bath which is of fundamental importance to describe the energy transport at finite temperature [28]. The paper is organized as follows. In Section 2, the two-site realization of the Davydov model is described and the key observables required to study the transport properties are introduced. In Section 3, we first establish the small polaron point of view and summarize the nature of the polaron quantum eigenstates. Then, the observables are redefined in this new point of view in terms of the polaron reduced density matrix. In Section 4, the polaron-phonon coupling is treated and a quantum kinetic equation for the reduced density matrix is established. This equation is solved numerically in Section 5 where a detailed analysis of the multi-quanta energy redistribution is performed. Finally, these results are discussed and interpreted in Section 6.

2 Description of the system

2.1 Model and Hamiltonians

Within the two-site realization of the Davydov model, we consider a dimer formed by two amide-I modes located at the sites $n = 0$ and $n = 1$ of a 1D lattice involving N sites which contain the peptide groups. The nth amide-I mode behaves as a high-frequency oscillator described by the standard vibron operators b_n^+ and b_n. The intramolecular anharmonicity is accounted through the model of Kimball et al. [20] so that the resulting vibron Hamiltonian H_v is expressed as (using the convention $\hbar = 1$),

$$H_v = \sum_{n=0,1} [\omega_0 b_n^\dagger b_n - A b_n^\dagger b_n^\dagger b_n b_n] + \Phi(b_0^\dagger b_1 + H.c.) \quad (1)$$

where H.c. denotes the Hermitian conjugate, ω_0 is the internal frequency of each amide-I mode, A is the positive anharmonicity parameter and Φ represents the vibron hopping constant between the two sites.

The dimer interacts with the phonons of the lattice which characterize the external motions of the peptide groups. They correspond to a set of N acoustic modes, labeled $\{q\}$, which the Hamiltonian is defined as

$$H_p = \sum_q \Omega_q a_q^\dagger a_q \quad (2)$$

where $a_q^\dagger$ and a_q are the phonon operators of the qth mode with frequency $\Omega_q = \Omega_c \mid \sin(q/2) \mid$, Ω_c denoting the phonon cutoff frequency.

Finally, the vibron-phonon interaction Hamiltonian characterizes a random modulation of the internal frequency of each amide-I mode as

$$\Delta H_{vp} = \sum_{qn} (\frac{\Delta_q}{\sqrt{N}} e^{-iqn} a_q^\dagger + \frac{\Delta_q^*}{\sqrt{N}} e^{iqn} a_q) b_n^\dagger b_n \quad (3)$$

where the coupling constant $\Delta_q = -2i\Delta_0 \sqrt{\mid \sin(q/2) \mid} \cos(q/2)$ is expressed in terms of the strength of the vibron-phonon coupling Δ_0.

2.2 Transport properties

Without any perturbation, the system is in thermal equilibrium at a temperature T at least equal to the room temperature. Therefore, since the relation $\hbar\omega_0 >> k_B T$ is fulfilled whatever T (k_B denotes the Boltzmann constant), only the ground state $\mid \Phi_g \rangle$ with zero vibron is significantly populated. This is no longer the case for the acoustic phonons ($\Omega_c << \omega_0$) for which the true eigenstates are not well defined. As a result, a statistical average is required by using the phonon density matrix ρ_p defined as

$$\rho_p = \frac{e^{-H_p/k_B T}}{Tr_p(e^{-H_p/k_B T})} \quad (4)$$

In that context, the energy transfer between the two amide-I results from the excitation of the dimer in a state out of equilibrium. To study this mechanism, we assume that under the coupling with an external source, V vibrons are initially created on the site $n = 0$. Consequently, the initial density matrix for

the whole system can be written as the tensorial product $\rho = \rho_v \otimes \rho_p$ where ρ_v is defined as

$$\rho_v = \frac{1}{V!} b_0^{\dagger V} \mid \Phi_g \rangle \langle \Phi_g \mid b_0^V \tag{5}$$

To characterize the vibrational energy flow, we introduce the vibron population $g_n(t) =< b_n^\dagger(t) b_n(t) >$ which represents the average value of the number of quanta on the nth site at time t. Since the full Hamiltonian conserves the vibron number, i.e. $g_0(t)+g_1(t) = V$ whatever t, only the population difference $\Delta g(t) = g_0(t) - g_1(t)$ is required. It is written as

$$\Delta g(t) = Tr[\rho e^{iHt}(b_0^\dagger b_0 - b_1^\dagger b_1)e^{-iHt}] \tag{6}$$

where the Trace defines an average over the initial condition specified by the density matrix ρ and the time evolution corresponds to an Heisenberg representation with respect to the full Hamiltonian $H = H_v + H_p + \Delta H_{vp}$.

The purpose of the present work is to study the time evolution of the population difference $\Delta g(t)$ depending on the number V of vibrons initially localized on the site 0. This evolution is governed by the full Hamiltonian H which cannot be solved exactly due to the anharmonicities. Therefore, the next section is devoted to its simplification through the introduction of the small polaron point of view.

3 Polaron point of view

3.1 Transformation and Hamiltonians

To describe the vibron dynamics in α-helices, the small polaron point of view has been used in several previous works. Here, we give a brief summary of the procedure and a detailed analysis can be found in Refs [11–17]. Therefore, to partially remove the vibron-phonon coupling Hamiltonian, a Lang-Firsov transformation [51] is applied so that the transformed Hamiltonian is written as

$$\hat{H} = \sum_n [\hat{\omega}_0 b_n^\dagger b_n - \hat{A} b_n^{\dagger 2} b_n^2] + E_B b_0^\dagger b_0 b_1^\dagger b_1 + \Phi(\Theta_0^\dagger \Theta_1 b_0^\dagger b_1 + H.c.) + H_p \tag{7}$$

where $\hat{\omega}_0 = \omega_0 - E_B$ and $\hat{A} = A + E_B$ are expressed in terms of the small polaron binding energy $E_B = 2\Delta_0^2/\Omega_c$ and where Θ_n stands for the dressing

operator defined as

$$\Theta_n = \exp[-\frac{1}{\sqrt{N}}\sum_{qn}(\frac{\Delta_q}{\Omega_q}e^{-iqn}a_q^\dagger - \frac{\Delta_q^*}{\Omega_q}e^{iqn}a_q)] \tag{8}$$

The next step of the procedure consists in expressing $\hat{H}$ as the sum of three separated contributions as $\hat{H} = H_{po} + H_p + \Delta H$. The polaron Hamiltonian H_{po}, obtained after performing a thermal average over the phonon degrees of freedom, is written as

$$H_{po} = \sum_n[\hat{\omega}_0 b_n^\dagger b_n - \hat{A}b_n^\dagger b_n^\dagger b_n b_n] + E_B b_0^\dagger b_0 b_1^\dagger b_1 + \hat{\Phi}(b_0^\dagger b_1 + H.c.) \tag{9}$$

where the effective hopping constant $\hat{\Phi} = \Phi\exp(-S(T))$ is expressed in terms of the coupling constant $S(T)$ defined as

$$S(T) = \sum_q \frac{4E_B}{N\Omega_c} \mid \sin(\frac{q}{2}) \mid \cos^2(\frac{q}{2})\coth(\frac{\Omega_q}{2k_BT}) \tag{10}$$

Finally, the remaining part of the polaron-phonon interaction ΔH is defined as

$$\Delta H = V_{01}b_0^\dagger b_1 + H.c. \tag{11}$$

where $V_{01} = \Phi[\Theta_0^\dagger\Theta_1 - < \Theta_0^\dagger\Theta_1 >_p]$

In this new point of view, the operators $b_n^\dagger$ and b_n define small polarons corresponding to vibrons dressed by a lattice distortion. The dressing prevents the delocalization of the polarons for which the effective hopping constant $\hat{\Phi}$ is smaller than the bare constant Φ. It yields a redshift of the vibrational frequency of each mode and produces additional anharmonicities characterizing the interaction between polarons due to the overlap between their virtual cloud of phonons. Finally, the polaron-phonon coupling remains through the modulation of the lateral term by the dressing operator fluctuations. Although these operators depend on the phonon coordinates in a highly nonlinear way, the interaction has been strongly reduced and a standard perturbation theory can be applied. This procedure requires the knowledge of the properties of the unperturbed dimer which are summarized in the next section.

As shown in Eq.(9), the Hamiltonian H_{po} commutes with the operator $\sum_n b_n^+ b_n$ which counts the total number of polarons. Therefore, the corresponding Hilbert space $\mathcal{E}$ is written as the tensor product $\mathcal{E} = \mathcal{E}_0 \otimes \mathcal{E}_1 \otimes ... \otimes \mathcal{E}_V ...$, where $\mathcal{E}_V$ is the subspace which describes V polarons. A useful basis set to generate the entire $\mathcal{E}_V$ subspace, whose dimension $V+1$, is defined as

$$\mid p\rangle_V = \frac{b_0^{\dagger p} b_1^{\dagger (V-p)}}{\sqrt{p!(V-p)!}} \mid \Phi_g\rangle \tag{12}$$

The vector $\mid p\rangle_V$, with $p = 0, 1, ..., V$, describes the localization of p and $V-p$ polarons on the sites 0 and 1, respectively. Note that we shall study the polaron dynamics after the initial creation of V quanta. Since the full Hamiltonian conserves the number of polarons, this dynamics is confined in the subspace $\mathcal{E}_V$. Therefore, the index V which is implied, will be omitted and the basis vectors will be simply labeled $\mid p\rangle \equiv \mid p\rangle_V$.

Within this basis set, the restriction of the polaron Hamiltonian to the subspace $\mathcal{E}_V$ is expressed as

$$H_{po}(p'p) = \epsilon_p \delta_{p'p} + \hat{\Phi}\sqrt{(p+1)(V-p)}\delta_{p'p+1} + \hat{\Phi}\sqrt{p(V-p+1)}\delta_{p'p-1} \tag{13}$$

where the diagonal part is $\epsilon_p = V\hat{\omega}_0 - V(V-1)\hat{A} + p(V-p)(2A+E_B)$. It represents the vibrational energy of the dimer when p and $V-p$ quanta are localized on the site 0 and 1, respectively. It is the sum of the energies of the pth and $(V-p)$th vibrational levels of the modes 0 and 1. Moreover, it accounts for the additional energy which results from the overlap between the virtual cloud of phonons dressing polarons located onto different sites. The off-diagonal part of the Hamiltonian couples nearest neighbor basis vectors. It characterizes processes in the course of which a single polaron is exchanged between the two sites of the dimer. Note that Eq.(13) clearly shows the invariance of the Hamiltonian under the reflection symmetry which transforms the state $\mid p\rangle$ into the state $\mid V-p\rangle$.

When a single polaron is excited, i.e. when $V=1$, the anharmonicity does not affect the quantum properties of the dimer. A resonance takes place between the basis vectors $\mid 0\rangle$ and $\mid 1\rangle$ which have the same energy $\epsilon_0 = \epsilon_1$. The polaron is thus delocalized between these two states so that the resulting eigenstates correspond to their symmetric and antisymmetric superimpositions. The energy splitting between the two eigenstates is equal to $2\hat{\Phi}$. For greater V values, a similar situation is recovered in the harmonic situation, i.e. $A=0$ and $E_B=0$. Since $\epsilon_p = V\omega_0$ whatever p, a resonance occurs between

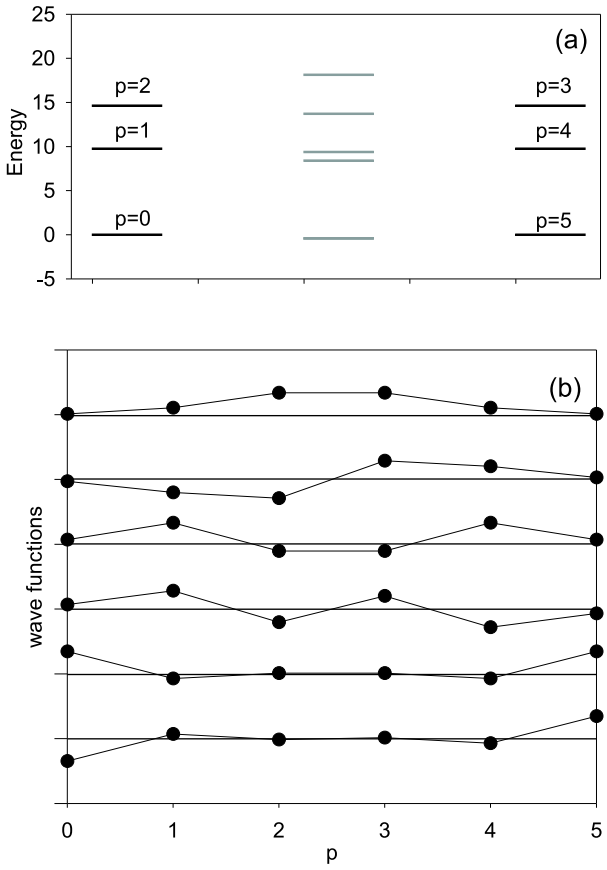

Fig. 1. Quantum states of the dimer for $V = 5$, $\Phi = 7.8$ cm^{-1}, $A = 8$ cm^{-1}, $E_B = 3$ cm^{-1}, $\Omega_c = 92$ cm^{-1} and $T = 100K$. (a) Black lines describe the energy levels in the limit $\Phi = 0$ whereas gray lines characterize the eigenvalues of the small polaron Hamiltonian. The energies, expressed in Φ unit, are centered onto ϵ_0. (b) Corresponding wave functions in the local basis set $\mid p\rangle$.

the different basis vectors. The eigenstates are delocalized over the entire basis set and the corresponding energy levels, centered around $V\hat{\omega}_0$, form a set of equidistant levels separated by 2Φ.

By contrast, excepted for the simple case $V = 2$, Eq.(13) cannot be solved analytically in the anharmonic situation and a numerical diagonalization is required. In Fig. 1, the nature of both the energy levels and the corresponding wave functions is illustrated for $V = 5$, $\Phi = 7.8$ cm^{-1}, $A = 8$ cm^{-1}, $E_B = 3$ cm^{-1}, $\Omega_c = 92$ cm^{-1} and $T = 100K$. The anharmonicity breaks the resonance between nearest neighbor $\mid p\rangle$ vectors and it produces localized states which basically keep the memory of the local basis set. More precisely, due to the reflection symmetry a resonance between the states $\mid p\rangle$ and $\mid V - p\rangle$ remains so that these two vectors tend to hybridize preferentially to create a symmetric and an antisymmetric superimpositions. The two lower levels clearly show a strong hybridization between $\mid 0\rangle$ and $\mid V\rangle$ which results in a very small energy splitting approximately expressed as (see for instance [46–50])

$$\Delta E = \frac{2V\hat{\Phi}^V}{(V-1)!(2A+E_B)^{V-1}} \tag{14}$$

These two states refer to V-polaron bound states delocalized between the two sites of the dimer. From a dynamical point of view, these bound states allow

for a coherent energy transfer between the two sites of the dimer which results in oscillations of the energy flow with a period of about ΔE^{-1}. The increase of this period with both anharmonicities and the number of quanta yields the quantum picture of the classical self-trapping. For greater p values, although the resonance $\epsilon_p = \epsilon_{V-p}$ favors the coupling between $\mid p\rangle$ and $\mid V-p\rangle$, nearest neighbor states $\mid p \pm 1\rangle$ and $\mid V - p \pm 1\rangle$ participate in the hybridization mechanism and they make easier the extension of the eigenstates over the entire local basis.

3.3 Reduced density matrix

Since the vibron number is conserved under the Lang-Firsov transformation, the vibron population is equal to the polaron population. As a consequence, in the new point of view, the time evolution is given by the Heisenberg representation with respect to the full Hamiltonian $\hat{H}$ (Eq.(7)) and the population difference between the two sites of the dimer is expressed as

$$\Delta g(t) = Tr[\hat{\rho} e^{i\hat{H}t}(b_0^\dagger b_0 - b_1^\dagger b_1)e^{-i\hat{H}t}] \tag{15}$$

where $\hat{\rho} = \rho_v \Theta_0^{\dagger V} \rho_p \Theta_0^V$ is the transformed initial density matrix. The polaron density matrix is equivalent to the vibron density matrix, i.e. $\rho_v = \mid V\rangle\langle V \mid$, whereas the phonon density matrix has been modified. Indeed, since a polaron in the new point of view corresponds to a vibron dressed by a lattice distortion, a vibron in the old point of view thus describes a polaron dressed by a local modification of the phonon field. As a consequence, the creation of V vibrons on the site 0 yields V polarons accompanied by a local disturbance of the phonon state. Therefore, the resulting phonon density matrix differs from the equilibrium distribution (Eq.(4)) and accounts for this local modification.

By introducing the local basis set $\{ \mid p\rangle \}$, the population difference is rewritten as

$$\Delta g(t) = \sum_{p=0}^{V} (2p - V)\sigma(p, p, t) \tag{16}$$

where $\sigma(p_1, p_2, t)$ is the reduced polaron density matrix at time t. It is defined as

$$\sigma(p_1, p_2, t) = Tr[\mid V\rangle\langle V \mid \Theta_0^{\dagger V} \rho_p \Theta_0^V e^{i\hat{H}t} \mid p_2\rangle\langle p_1 \mid e^{-i\hat{H}t}] \tag{17}$$

and it satisfies the initial condition $\sigma(p_1, p_2, 0) = \delta_{p_1,V}\delta_{p_2,V}$.

The reduced density matrix is the central object of the present study. It describes the polaron states at time t after performing the average over the phonon degrees of freedom. A diagonal element $\sigma(p,p,t)$ characterizes the population of the state $\mid p\rangle$. A non diagonal element $\sigma(p_1,p_2,t)$ measures the coherence between the two states $\mid p_1\rangle$ and $\mid p_2\rangle$ when the quantum state of the dimer is a superimposition of such states. The knowledge of the reduced density matrix allows us to compute in principle all the required observables to describe the energy flow in the dimer. Therefore, the following section is devoted to the derivation of a quantum kinetic equation to study its time evolution.

4 Quantum kinetic equation

In the polaron point of view, the initial density matrix for the whole system can be expressed as $\rho_v\rho_p\rho_c$ where $\rho_c = \rho_p^{-1}\Theta_0^{\dagger V}\rho_p\Theta_0^V$ denotes the correlation density matrix which depends on the phonon degrees of freedom only. It accounts for the difference between the initial phonon density matrix in the polaron point of view and the equilibrium distribution ρ_p (Eq.(4)). Therefore, in Eq.(17), the total trace can be splitted into partial traces Tr_{po} and Tr_p over the polaron and phonon degrees of freedom, respectively. As a consequence, within the Liouville space formalism [52], the reduced density matrix is rewritten as

$$\sigma(p_1,p_2,t) = Tr_{po}[\mid V\rangle\langle V \mid Tr_p[\rho_p\rho_c e^{i\hat{\mathcal{L}}t}] \mid p_2\rangle\langle p_1 \mid] \tag{18}$$

where $\hat{\mathcal{L}} = [\hat{H},...]$ is the Liouvillian associated to the full Hamiltonian.

To determine the time evolution of the reduced density matrix, we use the Zwanzig-Mori's projector technique [52–54] which has demonstrated its usefulness in eliminating irrelevant information from a system, i.e. the phonon dynamics in our case, and extracting only the information that is desired. Therefore, by performing a second order perturbation theory with respect to the polaron-phonon coupling ΔH (Eq. (11)), it is straightforward to show that the reduced density matrix satisfies the kinetic equation

$$\begin{aligned}\frac{\partial}{\partial t}\sigma(p_1,p_2,t) &= -i\sum_p [H_{po}(p_1,p)\sigma(p,p_2,t) - \sigma(p_1,p,t)H_{po}(p,p_2)] \\ &- \sum_{p_1',p_2'}\int_0^t d\tau \mathcal{J}(p_1,p_2;p_1',p_2',\tau)\sigma(p_1',p_2',t-\tau) + \mathcal{F}(p_1,p_2,t)\end{aligned} \tag{19}$$

where $\mathcal{J}(p_1,p_2;p_1',p_2',t)$ is the kernel memory defined as

$$
\begin{aligned}
&\mathcal{J}(p_1,p_2;p_1',p_2',t) = \\
&+\sum_{pp'}\langle\Delta H(p_1,p,t)\Delta H(p',p_1',0)\rangle_p G_{po}(p_2',p_2,-t)G_{po}(p,p',t) \\
&+\sum_{pp'}\langle\Delta H(p_2',p,0)\Delta H(p',p_2,t)\rangle_p G_{po}(p,p',-t)G_{po}(p_1,p_1',t) \\
&-\sum_{pp'}\langle\Delta H(p,p_2,t)\Delta H(p',p_1',0)\rangle_p G_{po}(p_2',p,-t)G_{po}(p_1,p_1',t) \\
&-\sum_{pp'}\langle\Delta H(p_2',p,0)\Delta H(p_1,p',t)\rangle_p G_{po}(p,p_2,-t)G_{po}(p',p_1',t)
\end{aligned}
\tag{20}
$$

and where $\mathcal{F}(p_1,p_2,t)$ denotes an initial force expressed as

$$
\begin{aligned}
&\mathcal{F}(p_1,p_2,t) = \\
&+i\sum p\langle\rho_c\Delta H(p,p_2,t)\rangle_p G_{po}(V,p,-t)G_{po}(p_1,V,t) \\
&-i\sum p\langle\rho_c\Delta H(p_1,p,t)\rangle_p G_{po}(V,p_2,-t)G_{po}(p,V,t)
\end{aligned}
\tag{21}
$$

In Eqs.(20) and (21), $\Delta H(p_1,p_2)$ is the representation of the coupling Hamiltonian ΔH in the basis set $\mid p\rangle$. It is an operator in the space of the phonon degrees of freedom, only, and its time dependence is obtained through an Heisenberg representation with respect to the phonon Hamiltonian H_p. The propagator $G_{po}(p_1,p_2,t)$ is the representation of the evolution operator $\exp(-iH_{po}t)$ which describes the free evolution of the unperturbed dimer.

In Eq.(19), the first term in the right-hand-side characterizes the coherent dynamics of the unperturbed polarons which corresponds to the free evolution of the reduced density matrix under the influence of the polaron Hamiltonian H_{po}. By contrast, the two other terms in the right-hand-side of Eq.(19) describe the influence of the coupling with the phonon bath. The kernel memory Eq.(20) represents the relaxation mechanisms. It accounts for the modification of the dynamics of the reduced density matrix at time t due to the history of the polaron-phonon coupling between $t = 0$ and t. The initial force Eq.(21), which vanishes when $\rho_c = 1$, originates in the initial statistical correlations between the polarons and the phonons.

In Eqs. (20) and (21), both the kernel memory and the initial force are expressed in terms of the correlation functions of the polaron-phonon coupling Hamiltonian. These correlation functions are characterized by the correlation time τ_c of the phonon bath which measures the time for which the correlations vanish. In a general way, τ_c is very short for low-dimensional molecular lattices and we have verified that it is about 0.5 ps in the present situation. Therefore, we assume that τ_c is shorter than the typical time governing the free evolution of the reduced density matrix, about the invert of the effective hopping constant, which is typically greater than 5 ps. As a consequence, this assumption allows us to invoke two simplifying approximations. First, we as-

sume that over a timescale of about τ_c, a polaron does not have enough time to realize a transition between the two sites of the dimer. The non diagonal elements of the free propagator $G_{po}(p_1, p_2, t)$ can thus be neglected in Eqs.(20) and (21). Then, the Markovian limit of the kinetic equation is assumed to be reached. Finally, the initial force will be disregarded because it produces only small perturbations in the evolution of the reduced density matrix in the very short time limit.

Therefore, these assumptions yield an approximated quantum kinetic equation for the reduced density matrix as

$$\frac{\partial}{\partial t}\sigma(t) = -i(\mathcal{L}_{po} - i\mathcal{R})\sigma(t) \tag{22}$$

where $\mathcal{L}_{po} = [H_{po}, ...]$ is the Liouvillian associated to the unperturbed dimer Hamiltonian and $\mathcal{R}$ is the relaxation operator which corresponds to the integration of the kernel memory. From the expression of the polaron-phonon coupling Hamiltonian (Eq.(11)), its representation in the basis set $\mid p\rangle$ is defined as

$$\begin{aligned}
&\mathcal{R}(p_1, p_2; p_1', p_2') = \\
&+ [\Gamma_{p_1+1,p_2}(p_1+1)(V-p_1) + \Gamma_{p_1-1,p_2}p_1(V-p_1+1)]\delta_{p_1',p_1}\delta_{p_2',p_2} \\
&+ [\Gamma^*_{p_2+1,p_1}(p_2+1)(V-p_2) + \Gamma^*_{p_2-1,p_2}p_2(V-p_2+1)]\delta_{p_1',p_1}\delta_{p_2',p_2} \\
&+ \gamma_{p_1+1,p_2}\sqrt{(p_1+1)(V-p_1)(p_1+2)(V-p_1-1)}\delta_{p_1',p_1+2}\delta_{p_2',p_2} \\
&+ \gamma^*_{p_2+1,p_1}\sqrt{(p_2+1)(V-p_2)(p_2+2)(V-p_2-1)}\delta_{p_1',p_1}\delta_{p_2',p_2+2} \\
&+ \gamma_{p_1-1,p_2}\sqrt{p_1(V-p_1+1)(p_1-1)(V-p_1+2)}\delta_{p_1',p_1-2}\delta_{p_2',p_2} \\
&+ \gamma^*_{p_2-1,p_1}\sqrt{p_2+(V-p_2+1)(p_2-1)(V-p_2+2)}\delta_{p_1',p_1}\delta_{p_2',p_2-2} \\
&- [\Gamma_{p_1,p_2+1} + \Gamma^*_{p_2,p_1+1}]\sqrt{(p_1+1)(V-p_1)(p_2+1)(V-p_2)}\delta_{p_1',p_1+1}\delta_{p_2',p_2+1} \\
&- [\Gamma_{p_1,p_2-1} + \Gamma^*_{p_2,p_1-1}]\sqrt{p_1(V-p_1+1)p_2(V-p_2+1)}\delta_{p_1',p_1-1}\delta_{p_2',p_2-1} \\
&- [\gamma_{p_1,p_2+1} + \gamma^*_{p_2,p_1-1}]\sqrt{p_1(V-p_1+1)(p_2+1)(V-p_2)}\delta_{p_1',p_1-1}\delta_{p_2',p_2+1} \\
&- [\gamma_{p_1,p_2-1} + \gamma^*_{p_2,p_1+1}]\sqrt{(p_1+1)(V-p_1)p_2(V-p_2+1)}\delta_{p_1',p_1+1}\delta_{p_2',p_2-1}
\end{aligned} \tag{23}$$

where the parameters Γ_{p_1,p_2} and γ_{p_1,p_2} are defined in terms of the integral of the correlation functions of the dressing operator fluctuations as (see Eq.(11))

$$\Gamma_{p_1,p_2} = \int_0^\infty \langle V_{01}(t)V_{10}(0)\rangle_p G_{po}(p_1, p_1, t)G^*_{po}(p_2, p_2, t)$$

$$\gamma_{p_1,p_2} = \int_0^\infty \langle V_{01}(t)V_{01}(0)\rangle_p G_{po}(p_1,p_1,t)G^*_{po}(p_2,p_2,t) \tag{24}$$

The relaxation operator accounts for the mixing between the different elements of the reduced density matrix mediated by the polaron-phonon coupling. It conserves the norm of the density matrix and it satisfies the sum rule $\sum_p \mathcal{R}(pp,p_1,p_2) = 0$. It contains all the physical information involved in the phase relaxation responsible for the return to a quasi-equilibrium. Indeed, since the coupling with the phonon bath conserves the vibron number, it accounts for dephasing mechanism only and does not allow for energy relaxation. Therefore, the quasi-equilibrium corresponds to a stationary solution for which the vibron number is equal to V. This solution differs from the thermal equilibrium which is assumed to occur over a timescale of about several orders of magnitude greater than the dephasing time. In fact, the quasi-equilibrium describes a situation in which the random fluctuations of the phonon bath have destroyed the quantum coherences in the dimer so that the density matrix becomes diagonal.

Therefore, Eq.(22) shows that the dynamics of the dimer is governed by the effective Liouvillian $\mathcal{L}_{eff} = \mathcal{L}_{po} - i\mathcal{R}$ which describes both the coherent energy transfer and the relaxation mechanisms. In the subspace $\mathcal{E}_V$, it is a tetradic operator represented by a $((V+1)^2 \times (V+1)^2)$ matrix which the diagonalization leads to $(V+1)^2$ complex eigenvalues λ_η and eigenvectors $\Psi_\eta(p_1,p_2)$ labeled by the index η. Form Eq.(22), the reduced density matrix is thus expressed in terms of the characteristics of the effective Liouvillian as

$$\sigma(p_1,p_2,t) = \sum_\eta \Psi_\eta(p_1,p_2)\Psi^*_\eta(V,V)e^{-i\lambda_\eta t} \tag{25}$$

Finally, by inserting Eq.(25) in Eq.(16), the population difference between the two site of the dimer can be expanded in terms of the effective Liouvillian eigenvectors. Due to the reflection symmetry of the dimer, the population difference is thus written as

$$\Delta g(t) = \sum_\eta \sum_{p=0}^{\frac{V}{2}} (V-2p)[\sigma_\eta(V-p,V-p) - \sigma_\eta(p,p)]e^{-i\lambda_\eta t} \tag{26}$$

where $\sigma_\eta(p_1,p_2) = \Psi_\eta(p_1,p_2)\Psi^*_\eta(V,V)$ and where the sum over p extends to the integer value of the ratio V/2.

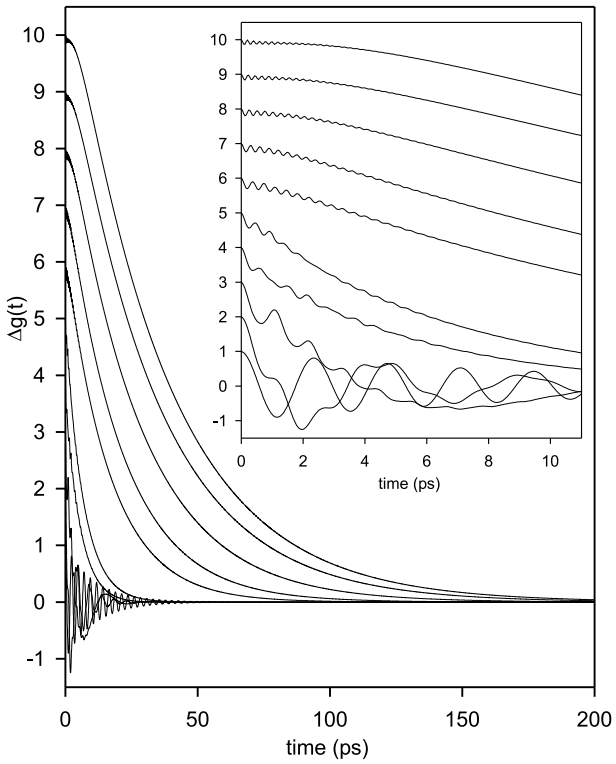

Fig. 2. Time evolution of the population difference $\Delta g(t)$ for $\Phi = 7.8$ cm^{-1}, $A = 8$ cm^{-1}, $E_B = 3$ cm^{-1}, $\Omega_c = 92$ cm^{-1}, $T = 100K$ and for $V = 1, 2, ..., 10$.

5 Numerical results

In this section, the previous formalism is applied to study the time evolution of the population difference $\Delta g(t)$. To proceed, the parameters Γ_{p_1,p_2} and γ_{p_1,p_2}, required to build the relaxation operator (Eq.(23)), are first evaluated using a numerical integration. Then, the effective Liouvillian is calculated and its numerical diagonalization is performed. From the knowledge of the corresponding eigenvalues and eigenvectors, the population difference is finally computed by using Eq.(26). These calculations are carried out using typical values for the relevant parameters involved in the theory. The vibron hopping constant is fixed to the well admitted value $\Phi = 7.8$ cm^{-1} [22,11] and the intramolecular anharmonicity is $A = 8.0$ cm^{-1} [13,29]. The phonon cutoff frequency is equal to $\Omega_c = 92$ cm^{-1} and the small polaron binding energy is fixed to $E_B = 3$ cm^{-1}.

The time evolution of the population difference is illustrated in Fig. 2 for $T = 100$ K and $V = 1, 2, ..., 10$. When $V = 1$, $\Delta g(t)$ exhibits damped oscillations revealing a coherent energy transfer between the two sites of the dimer. The frequency of these oscillations, about 14.04 cm^{-1}, is very close to $2\hat{\Phi}$. They are exponentially damped with a damping time equal to 11 ps. As a result, the population difference tends to zero so that the equilibrium corresponds to a uniform energy distribution over the two sites of the dimer. When $V = 2$, a coherent energy transfer remains and the population difference shows low-frequency damped oscillations which converge to the equilibrium. This

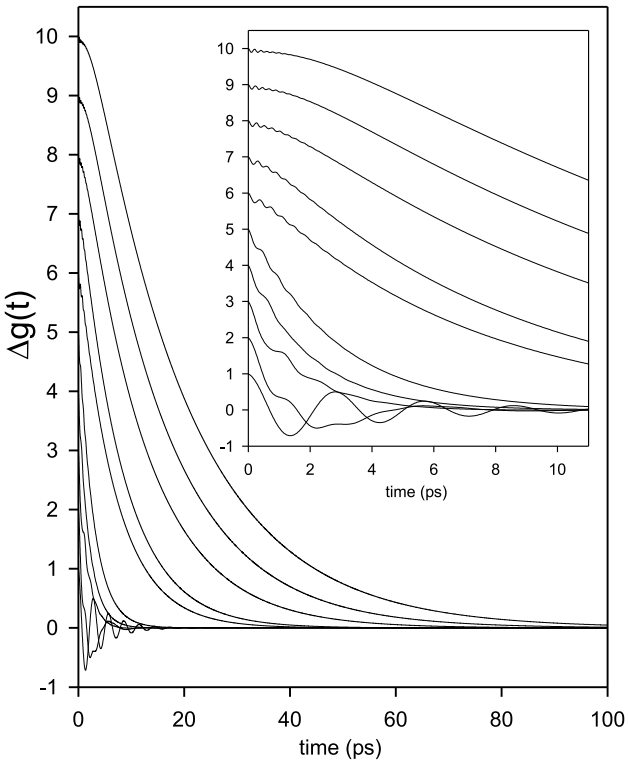

Fig. 3. Time evolution of the population difference $\Delta g(t)$ for $\Phi = 7.8$ cm^{-1}, $A = 8$ cm^{-1}, $E_B = 3$ cm^{-1}, $\Omega_c = 92$ cm^{-1}, $T = 300K$ and for $V = 1, 2, ..., 10$.

behavior is characterized by a frequency equal to 7.02 cm^{-1} and a damping time of about 5 ps. However, $\Delta g(t)$ exhibits a small amplitude modulation which the frequency is about 26.5 cm^{-1}. When $V = 3$, $\Delta g(t)$ behaves as previously and the coherent energy transfer is characterized by a frequency and a damping time equal to 1.96 cm^{-1} and 5.2 ps, respectively. The population difference supports a high-frequency modulation with a frequency about 29 cm^{-1} and which disappears over a timescale of about 2.8 ps. Finally, when $V = 4$ and 5, $\Delta g(t)$ still exhibits a damped coherent energy transfer with a damping time equal to 5.2 ps and 6.6 ps, respectively. However, the corresponding low frequencies are to small to be observed whereas the high-frequency small amplitude modulations in the short time limit appear clearly.

In a marked contrast, a fully different behavior occurs when $V \geq 6$. The population difference is always positive and it does not exhibit low-frequency oscillations. In the short time limit, the exponential damping has disappeared so that $\Delta g(t)$ slightly decreases from its initial value over a timescale which increases with V. It supports a small amplitude modulation which the frequency increases with V. For instance, this frequency is equal to 90 cm^{-1} when $V = 6$ and it reaches 169 cm^{-1} when $V = 10$. In the long time limit, $\Delta g(t)$ returns to the equilibrium according to a purely exponential decay which the damping time increases with V. When $V = 6$, this damping time is equal to 15.6 ps whereas it reaches 36.4 ps when $V = 10$, i.e. about one order of magnitude greater than the damping time observed for $V < 6$. This feature indicates that the larger is the number of polaron, the slower is the energy transfer between the two sites of the dimer.

As shown in Fig. 3, the same features occur when $T = 300$ K and a transition which discriminates between two dynamical regimes still remains when V ranges between 5 and 6. However, the increase of the temperature is responsible for a decrease of the different damping times. Therefore, both the return to the equilibrium and the damping of the small amplitude high-frequency modulation occur over a shorter timescale. In addition, the frequency of the coherent energy transfer is reduced.

To understand these features, a detailed analysis of the eigenvalues of the effective Liouvillian is displayed in Fig. 4. For each V value, the spectrum shows $(V+1)^2$ complex eigenvalues $\lambda_\eta = \lambda'_\eta - i\lambda''_\eta$ represented by a point which the coordinates are $(\lambda'_\eta, \lambda''_\eta)$. Several general properties are observed. First, the imaginary part of each eigenvalue is always negative ($\lambda''_\eta \geq 0$ whatever η). This feature ensures the convergence of the population difference in the long time limit. Then, each spectrum exhibits a set S_0 containing the eigenvalues which the real part vanishes, i.e. $S_0 = \{\lambda_\eta | \lambda'_\eta = 0\}$. Its dimension is at least equal to $(V+1)$, i.e. the number of eigenstates of the unperturbed dimer. Among the eigenvalues belonging to S_0, a single one vanishes exactly. It characterizes the equilibrium distribution. Finally, the eigenvalues which do not belong to S_0 can be grouped into pairs connected to two eigenvalues with the same imaginary part but with opposite real part.

From the comparison with the results displayed in Fig. 2, Fig. 4 clearly shows that when $V < 6$ the low-frequency damped coherent energy transfer is described by the two complementary eigenvalues with the smallest non vanishing real part in absolute value. Indeed, in a perfect agreement with the measurement obtained form Fig. 2, the spectrum yields frequencies equal to 14.06 cm^{-1}, 7.20 cm^{-1} and 2.01 cm^{-1} when $V = 1, 2$ and 3, respectively. For $V = 4$ and 5, the spectrum gives the frequencies 0.18 cm^{-1} and 0.07 cm^{-1} which were not measured in Fig. 2 due to their small values. Note that the imaginary part of the corresponding eigenvalues defines the damping rate in a perfect agreement with those observed in Fig. 2. These results show that as when V increases, the smallest non vanishing real part in absolute value decreases to finally vanishes when $V \geq 6$. In other words, when $V < 6$, the dimension of S_0 is equal to $(V+1)$ whereas it becomes greater than $(V+1)$ when $V \geq 6$. This process explains the disappearance of the coherent energy transfer since, when $V \geq 6$, the dynamics is governed by the eigenstates belonging to the set S_0 which do not produce oscillations.

At this step, the knowledge of the eigenvalues of the effective Liouvillian is insufficient to clearly understand the dynamics and a detailed analysis of the corresponding eigenstates must be performed. However, since a complete presentation cannot be done in the present paper, we shall restrict our attention to the specific eigenvectors $\sigma_\eta(p_1, p_2)$ which govern the short time and the long time limit of $\Delta g(t)$ (see Eq.(26)).

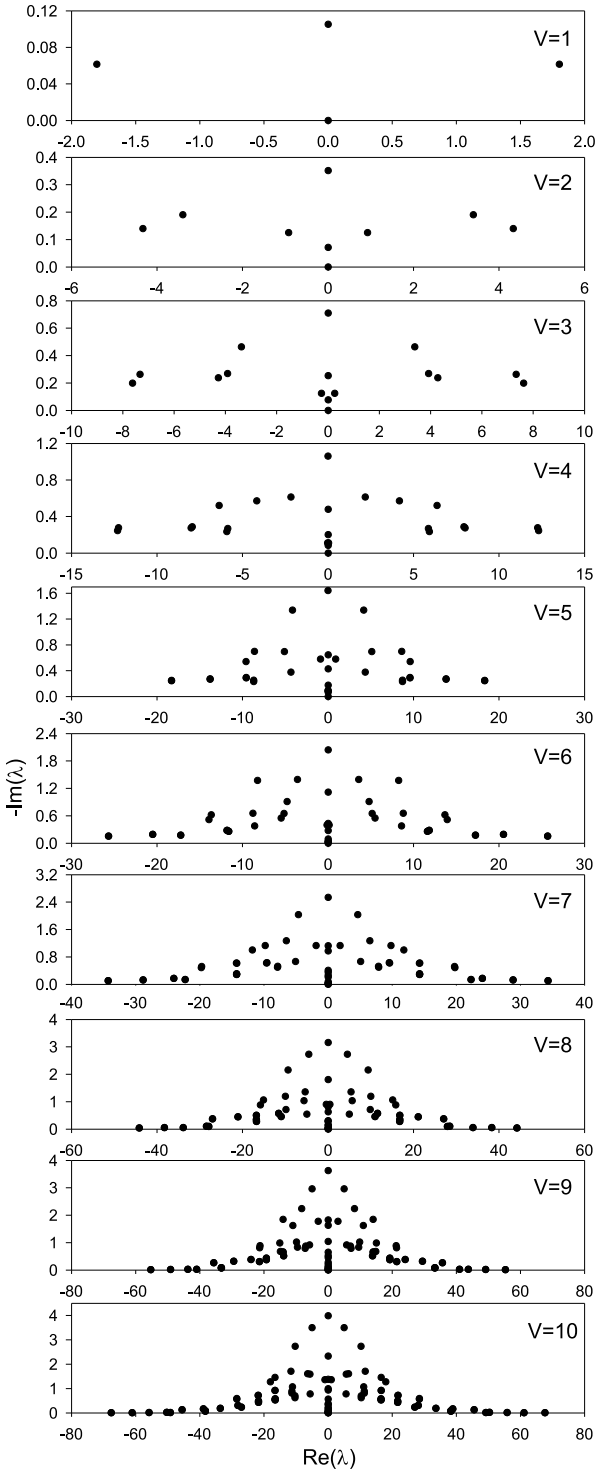

Fig. 4. Spectrum of the effective Liouvillian for $\Phi = 7.8$ cm^{-1}, $A = 8$ cm^{-1}, $E_B = 3$ cm^{-1}, $\Omega_c = 92$ cm^{-1}, $T = 100K$ and for $V = 1, 2, ..., 10$.

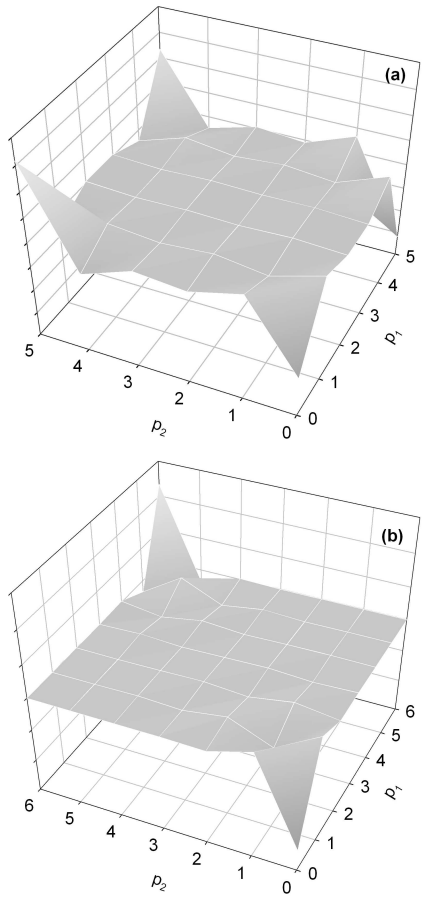

Fig. 5. Specific eigenstates of the effective Liouvillian responsible for the return the equilibrium for (a) $V = 5$, $\lambda = \pm 0.07 - i0.72$ cm^{-1} and (b) $V = 6$, $\lambda = -i0.32$ cm^{-1}.

In the long time limit, the return to the equilibrium is characterized by an exponential decreases of $\Delta g(t)$, with or without oscillations, depending on the value of the number of quanta. Eq.(26) shows that this dynamics is governed by the eigenstates with the smallest non vanishing damping rate λ''_η and with the largest $\sigma_\eta(V-p,V-p) - \sigma_\eta(p,p)$ value. However, since the most important contribution to $\Delta g(t)$ is carried by $\sigma_\eta(V,V) - \sigma_\eta(0,0)$ and since the eigenstates are symmetric or antisymmetric due to the reflection symmetry of the dimer, we conclude that the return to the equilibrium is governed by the antisymmetric eigenstates which maximize $\sigma_\eta(V,V)$. Therefore, our analysis has reveled the existence of a transition between two kind of eigenstates depending on the V value. When $V < 6$ (Fig. 5a), the long time behavior is governed by two antisymmetric eigenstates with complementary eigenvalues $\pm\lambda'_\eta - i\lambda''_\eta$. Their most important components involve the populations $\sigma_\eta(V,V)$ and $\sigma_\eta(0,0)$ as well as the coherences $\sigma_\eta(0,V)$ and $\sigma_\eta(V,0)$. Since $\lambda'_\eta \neq 0$, they yield coherent oscillations with a damping rate equal to λ''_η. By contrast, when $V \geq 6$ (Fig. 5b), the return to the equilibrium is governed by a single antisymmetric eigenstate associated to a purely imaginary eigenvalue $-i\lambda''_\eta$. This state involves mainly the two populations $\sigma_\eta(V,V)$ and $\sigma_\eta(0,0)$ and, to a lesser extent, the other populations $\sigma_\eta(V-1,V-1)$, $\sigma_\eta(V-2,V-2)$ ... as well as the coherences $\sigma_\eta(V,V-1)$, $\sigma_\eta(V-1,V-2)$ ... Since $\lambda'_\eta = 0$, it yields an

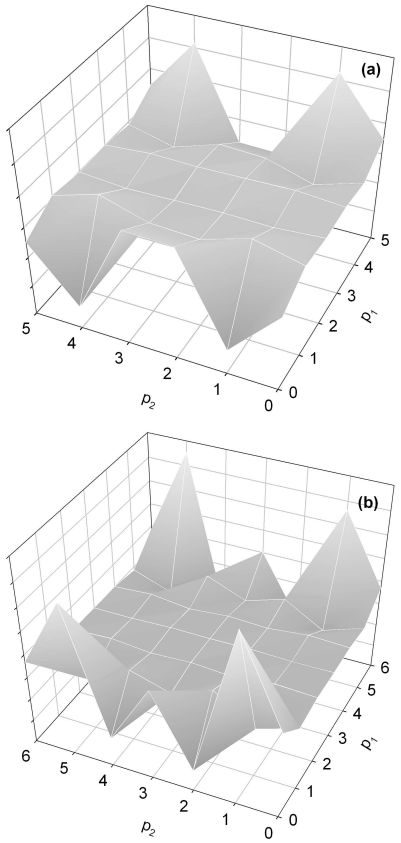

Fig. 6. Specific eigenstates of the effective Liouvillian which govern the short time behavior of the population difference for (a) $V = 5$, $\lambda = \pm 67.94 - i1.97$ cm^{-1} and (b) $V = 6$, $\lambda = \pm 92.19 - i2.18$ cm^{-1}.

exponential damping without oscillation and with a damping rate equal to λ''_η.

Since V quanta are initially created onto the site 0, the short time behavior of $\Delta g(t)$ is governed by the population $\sigma(V, V, t)$. Therefore, the eigenstates which participate in the short time evolution maximize $\sigma_\eta(V, V)$. Among the required eigenvectors, we recover the eigenstates responsible for the long time dynamics as well as the eigenstate which describes the equilibrium. However, other specific eigenstates associated to eigenvalues with a large real part seem to play a key role. As illustrated in Figs. 6, these states involve mainly the coherence $\sigma_\eta(V, V-1)$ although $\sigma_\eta(0, 1)$, $\sigma_\eta(V, 1)$, and $\sigma_\eta(0, V-1)$ participate due to the reflection symmetry. As a consequence, whatever the value of V, the short time dynamics results from the coherent superimposition of the states $\mid V\rangle$ and $\mid V-1\rangle$ which yields oscillations with a high-frequency of about $\epsilon_{V-1} - \epsilon_V$, in a perfect agreement with the observations shown in Fig. 2.

In Fig. 7, the behavior of the long time decay rate is displayed for different V values and for $T = 100$ K (Fig. 7a) and $T = 300$ K (Fig. 7b). This decay rate is the imaginary part of the eigenvalue of the effective Liouvillian associated to the eigenstate responsible for the return to the equilibrium. Open circles correspond to numerical results whereas full circles describe theoretical calculations which will be introduced in the next section. The situation $V = 1$ is rather specific and it is characterized by a small rate equal to 0.48 cm^{-1} and

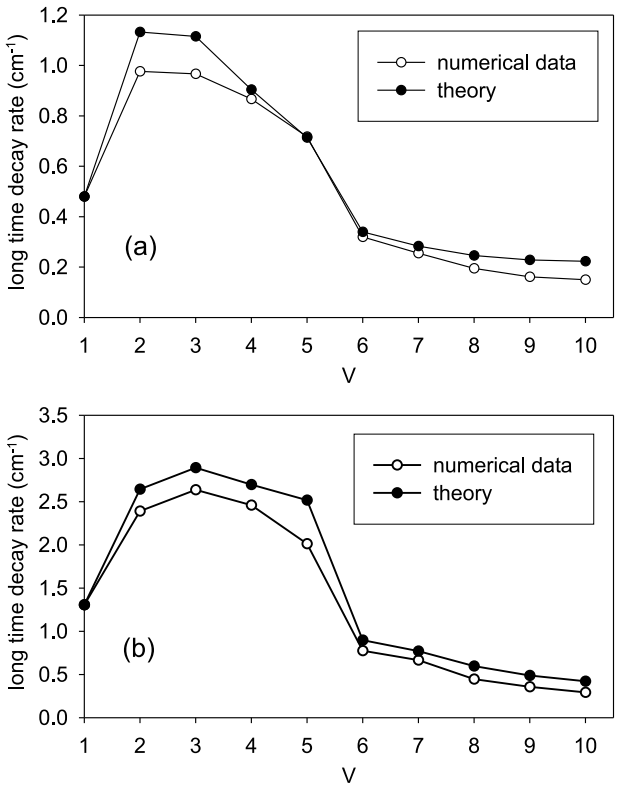

Fig. 7. Long time decay rate vs the number of quanta (a) $T = 100$ K and (b) $T = 300$ K. Open circles correspond to numerical results whereas full circles describe theoretical calculations

1.30 cm^{-1}, when $T = 100$ K and $T = 300$ K, respectively. When V ranges between 2 and 5, the decay rate varies slowly around 0.87 cm^{-1} when T=100 K and around 2.37 cm^{-1} when T=300 K. Then, a transition takes place since the decay rate is clearly reduced of about one order of magnitude when $V \geq 6$. It decreases with the number of quanta and it reaches 0.15 cm^{-1} at $T = 100$ K and 0.29 cm^{-1} at $T = 300$ K when $V = 10$. These results corroborate the observations made in Figs. 2 and 3 and they clearly show the occurrence of a transition in the way the dimer returns to the equilibrium.

The behavior of $\Delta g(t)$ for $A = 2, 4, ..., 20$ cm^{-1} is illustrated in Fig. 8 for $T = 100$ K and $V = 5$. The transition between the two dynamical regimes is observed depending on the value of the anharmonicity for a fixed V value. This transition takes place when A typically ranges between 10 and 11 cm^{-1}. Indeed, when $A = 2, 4, ..., 10$ cm^{-1}, a detailed analysis of Fig. 8 reveals that $\Delta g(t)$ exhibits low-frequency damped oscillations to finally converges to the equilibrium. In addition, in the short time limit, the exponential decreases of $\Delta g(t)$ supports a high-frequency small amplitude modulation which both the amplitude and the damping time decreases with the anharmonicity. By contrast, when $A = 12, 14, ..., 10$ cm^{-1}, a purely incoherent motion takes place without any low-frequency oscillations. In the long time limit, the return to the equilibrium is ensured by an exponential decay which the damping rate

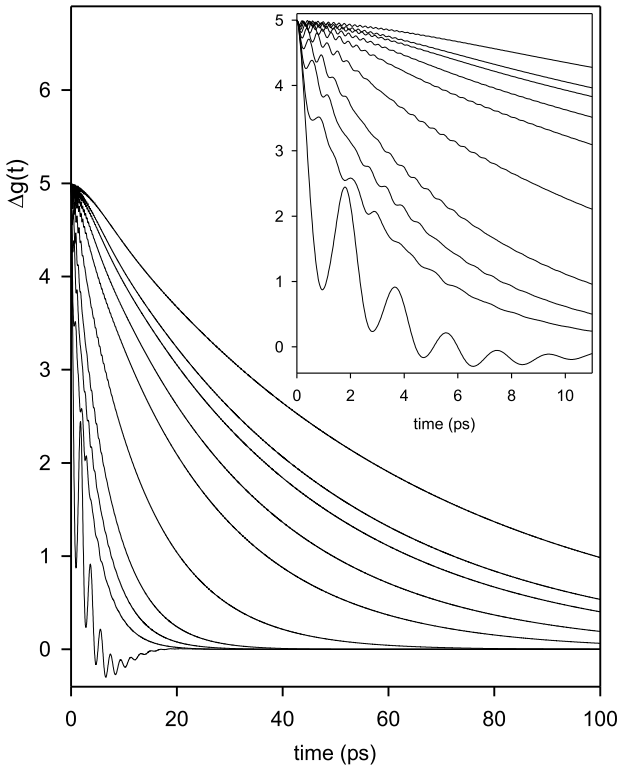

Fig. 8. Time evolution of the population difference $\Delta g(t)$ for $V = 5$, $\Phi = 7.8$ cm^{-1}, $E_B = 3$ cm^{-1}, $\Omega_c = 92$ cm^{-1}, $T = 300K$ and for $A = 2, 4, 6, ..., 20$ cm^{-1}.

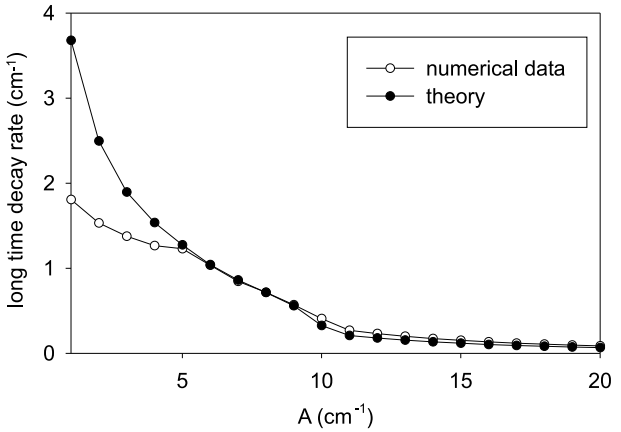

Fig. 9. Long time decay rate vs the anharmonicity for $V = 5$. (a) $T = 100$ K and (b) $T = 300$ K. Open circles correspond to numerical results whereas full circles describe theoretical calculations

decreases with A. In the short time limit, $\Delta g(t)$ decreases very slowly over a timescale which increases with A and it supports a high-frequency small amplitude modulation which the frequency increases with A.

Finally, Fig. 9 shows the behavior of the long time decay rate for different A values and for $V = 5$ and $T = 100$ K. Open circles correspond to numerical results whereas full circles describe theoretical calculations. A transition takes place for A about 11 cm^{-1}, in a perfect correspondence with the results obtained in Fig. 8. When $A < 11$ cm^{-1}, the decay rate exhibits important value but it decreases rapidly with the anharmonicity to reach a second regime when

$A > 11$ cm^{-1}. In this latter case, the decay rate varies rather slowly although it still decreases with the anharmonicity.

6 Interpretation and discussion

In the previous section, our numerical results have revealed the existence of a transition between two dynamical regimes for the population difference. This transition occurs depending on the value of either the number of quanta V or the anharmoncity A. In fact, as it will be shown in this section, the transition mainly depends on the structure of the energy spectrum of the dimer when compared with that of the phonon bath. Therefore, below the critical value V^* (or A^*), the population difference exhibits low-frequency oscillations revealing a coherent energy transfer between the two sites of the dimer. These oscillations are exponentially damped so that they converge to an equilibrium configuration in which the vibrational energy is uniformly distributed over the two sites. In addition, excepted for $V = 1$, the population difference supports a high-frequency small amplitude contribution which modulates its exponential decay in the short time limit. Our analysis has revealed that the energy transfer originates in a strong coherence between the states $\mid V\rangle$ and $\mid 0\rangle$ which participate in the formation of the quantum state involving their superimposition. However, the short time behavior results from the superimposition of the states $\mid V\rangle$ and $\mid V-1\rangle$ which produces a high-frequency coherence responsible for the modulation of the population difference. By contrast, above the critical value V^* (or A^*), a purely incoherent motion takes place without any low-frequency oscillations. The return to the equilibrium is ensured by an exponential decrease characterized by a very small decay rate. However, in the short time limit, the population difference decreases very slowly over a few picoseconds and exhibits a high-frequency small amplitude modulation which, as previously, results from the superimposition of the states $\mid V\rangle$ and $\mid V-1\rangle$.

6.1 General formulation

To interpret the numerical results, a projection technique is introduced to evaluate the behavior of the population difference. This method, which is exact when $V = 1$, allows us to realize relevant approximations to understand the general situation occurring when $V \geq 2$. To proceed, let us introduce the Liouville space formalism described in details in Ref. [52]. When V polarons are excited, the Liouville space is defined as the tensorial product $\mathcal{L}_V = \mathcal{E}_V \otimes \mathcal{E}_V^\dagger$. Therefore, the basis set $\{ \mid p\rangle \}$ allows to build the operators $\mid p_1\rangle\langle p_2 \mid$ which can be viewed as a set of $(V+1)^2$ vectors, denoted $\mid p_1, p_2^\dagger\rangle\rangle$, and which form a

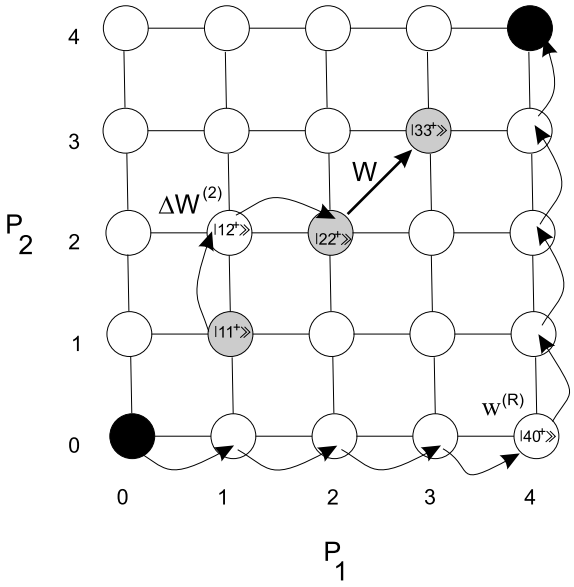

Fig. 10. Liouville space for V=4. Black, gray and white circles denote the populations $\mid V, V^\dagger\rangle\rangle$ and $\mid 0, 0^\dagger\rangle\rangle$, the other populations and the coherences, respectively. W defines hops due to the energy exchange with the bath. $\Delta W^{(2)}$ and $w^{(R)}$ describe transitions mediated by the coupling with the coherences (see the text).

useful basis to generate $\mathcal{L}_V$ (see Fig. 10). In this context, the reduced density matrix $\sigma(p_1, p_2, t)$ is the projection of a vector $\mid \sigma(t)\rangle\rangle$. Its time evolution is governed by the effective Liouvillian as

$$\sigma(p_1, p_2, t) = \langle\langle p_1^\dagger, p_2 \mid e^{-i\mathcal{L}_{eff}t} \mid V, V^\dagger\rangle\rangle \tag{27}$$

where the initial condition $\mid \sigma(0)\rangle\rangle = \mid V, V^\dagger\rangle\rangle$ has been used. By first performing the Laplace transform of Eq.(27), and then by inserting the obtained result into the expression of the population difference, the Laplace transform of $\Delta g(t)$ is defined as

$$\Delta\tilde{g}(z) = \sum_{p=0,V} (2p - V)\langle\langle p^\dagger, p \mid G(z) \mid V, V^\dagger\rangle\rangle \tag{28}$$

where z is the Laplace variable and $G(z)$ is the Green operator defined as

$$G(z) = (z + i\mathcal{L}_{eff})^{-1} \tag{29}$$

Because of the complex nature of the effective Liouvillian, Eq.(28) cannot be solved exactly when $V \geq 2$. However, as it will be shown in the following of the text, a full description of the population difference is not required to understand the observed features. Therefore, we restrict our attention to the main contribution of Eq.(28), still exact when $V = 1$ and defined as

$$\Delta\tilde{g}(z) \approx V[\langle\langle V^\dagger, V \mid G(z) \mid V, V^\dagger\rangle\rangle - \langle\langle 0^\dagger, 0 \mid G(z) \mid V, V^\dagger\rangle\rangle] \tag{30}$$

Eq.(30) shows that $\Delta\tilde{g}(z)$ only depends on the restriction of the Green operator to the subspace containing the populations $\mid 0, 0^\dagger\rangle\rangle$ and $\mid V, V^\dagger\rangle\rangle$. To

determine this restriction, a two step projection technique is used in which we first focus our attention onto the subspace containing all the populations and then perform a projection onto the two required populations. To proceed, let P denotes the projector onto the set of the populations. Since a single index is required to describe the subset $\{\mid p, p^\dagger\rangle\rangle\}$, the restriction $PG(z)P$ is represented by a $((V+1)\times(V+1))$ matrix as

$$PG(z)P = \frac{P}{z + W + \Delta W(z)} \tag{31}$$

where $W = iP\mathcal{L}_{eff}P$. Since $\mathcal{L}_{po}$ couples populations to coherences, only, its restriction vanishes, i.e. $P\mathcal{L}_{po}P = 0$. Therefore, W reduces to the projection $P\mathcal{R}P$ of the relaxation operator. The diagonal element $W_{pp} = \mathcal{R}(pp, pp)$ describes the full transition rate to leave incoherently the state $\mid p\rangle$ due to the coupling with the phonon bath. In the same way, the non diagonal element $W_{pp'} = \mathcal{R}(pp, p'p')$ is the opposite of the rate for the transition between $\mid p\rangle$ and $\mid p'\rangle$ (see Fig. 10). The elements of W are written as

$$W_{pp'} = \delta_{p'p}(W_{p\to p+1} + W_{p\to p-1}) - \delta_{p'p+1}W_{p+1\to p} - \delta_{p'p-1}W_{p-1\to p} \tag{32}$$

where the rate $W_{p'\to p}$ is defined as (see Eq.(23))

$$W_{p'\to p} = 2Re[\Gamma_{p,p+1}(p+1)(V-p)\delta_{p',p+1} + \Gamma_{p,p-1}p(V-p+1)\delta_{p',p-1}] \tag{33}$$

In Eq.(31), the operator $\Delta W(z)$ is expressed in terms of the projector $Q = 1 - P$ onto the coherences $\mid p_1^\dagger, p_2\rangle\rangle$ $(p_1 \neq p_2)$ as

$$\Delta W(z) = P\mathcal{L}_{eff}Q(z + iQ\mathcal{L}_{eff}Q)^{-1}Q\mathcal{L}_{eff}P \tag{34}$$

It describes transitions between the different states $\mid p\rangle$ which result from the ability of the effective Liouvillian to produce quantum states as coherent superimpositions of the local basis vectors. In such a superimposition, coherences occur between the different basis vectors so that, in the Liouville space picture, population-population interaction takes place mediated by the population-coherence coupling. As for W, the diagonal elements of $\Delta W(z)$ characterize the rates to leave a given state whereas non diagonal elements define the opposite of the transition rates connecting two basis vectors (see Fig. 10).

The next step of our procedure consists in defining the projector $\mathcal{P}$ onto the populations $\mid 0, 0^\dagger\rangle\rangle$ and $\mid V, V^\dagger\rangle\rangle$. After some algebraic manipulations, the

restriction $\mathcal{P}G(z)\mathcal{P}$ is written as

$$\mathcal{P}G(z)\mathcal{P} = \frac{\mathcal{P}}{z + \mathcal{W}(z)} \tag{35}$$

where $\mathcal{W}(z)$ is expressed in terms of the projector $\mathcal{Q} = 1 - \mathcal{P}$ onto the remaining populations $\mid p, p^{\dagger}\rangle\rangle$, $0 < p < V$, as

$$\begin{aligned} \mathcal{W}(z) &= \mathcal{P}(W + \Delta W(z))\mathcal{P} \\ &- \mathcal{P}(W + \Delta W(z))\mathcal{Q}(z + \mathcal{Q}(W + \Delta W(z))\mathcal{Q})^{-1}\mathcal{Q}(W + \Delta W(z))\mathcal{P} \end{aligned} \tag{36}$$

The operator $\mathcal{W}(z)$ is represented by a (2×2) matrix which contains the effective transition rates describing the population exchanges between the two states $\mid 0\rangle$ and $\mid V\rangle$. The first term in the right-hand-side of Eq.(36) accounts for a direct population exchange mediated by the full transition rate operator $W + \Delta W(z)$. By contrast, the second term in the right-hand-side of Eq.(36) describes population exchanges between $\mid 0\rangle$ and $\mid V\rangle$ through their coupling with the other populations. Due to the reflection symmetry, the states $\mid 0\rangle$ and $\mid V\rangle$ are equivalent so that $\mathcal{W}_{00}(z) = \mathcal{W}_{VV}(z)$ and $\mathcal{W}_{0V}(z) = \mathcal{W}_{V0}(z)$. Therefore, by inserting Eq.(35) into Eq.(30), the Laplace transform of the population difference is finally written as

$$\Delta\tilde{g}(z) \approx \frac{V}{z + \mathcal{W}_{00}(z) - \mathcal{W}_{0V}(z)} \tag{37}$$

Eq.(37) clearly shows that the effective transition rate matrix $\mathcal{W}(z)$ is the central object of our analysis. Its knowledge allows to understand the different mechanisms responsible for the energy exchanges between $\mid 0\rangle$ and $\mid V\rangle$ and finally to compute the population difference. These calculations are illustrated in the next sections in both the simple case $V = 1$ and in the general situation $V \geq 2$.

6.2 Exact results for $V = 1$

When $V = 1$, the Liouville space contains the populations $\mid 0, 0^{\dagger}\rangle\rangle$ and $\mid 1, 1^{\dagger}\rangle\rangle$ and the coherences $\mid 0, 1^{\dagger}\rangle\rangle$ and $\mid 1, 0^{\dagger}\rangle\rangle$. As a consequence, the projectors $\mathcal{P}$ and P are equivalent so that the effective transition rate matrix Eq.(36) reduces to $\mathcal{W}(z) = W + \Delta W(z)$.

From the expression of the relaxation operator Eq.(23), the (2×2) matrix

which describes the incoherent transition rates is written as

$$W = w \begin{pmatrix} 1 & -1 \\ -1 & 1 \end{pmatrix} \tag{38}$$

where $w = W_{0\to 1} = 2Re\Gamma_{00}$ denotes the incoherent transition rate between $\mid 0\rangle$ and $\mid 1\rangle$.

Because of the reflection symmetry, the states $\mid 0\rangle$ and $\mid 1\rangle$ are equivalent so that they are characterized by the same energy $\epsilon_0 = \epsilon_1$. Therefore, the restriction of the small polaron Liouvillian to the coherences $\mid 0, 1^\dagger\rangle\rangle$ and $\mid 1, 0^\dagger\rangle\rangle$ vanishes. In addition, since the relaxation operator does not couple populations and coherences, i.e. $P\mathcal{R}Q = 0$ when $V = 1$, the operator $\Delta W(z)$ reduces to

$$\Delta W(z) = \mathcal{P}\mathcal{L}_{po}Q(z + Q\mathcal{R}Q)^{-1}Q\mathcal{L}_{po}\mathcal{P} \tag{39}$$

where $Q\mathcal{R}Q$ is the restriction of the relaxation operator to the coherence subspace defined as (see Eq.(23))

$$Q\mathcal{R}Q = \begin{pmatrix} \Gamma & -\gamma \\ -\gamma & \Gamma \end{pmatrix} \tag{40}$$

The constant $\Gamma = \Gamma_{11} + \Gamma_{00}^*$ characterizes the dephasing mechanism in the course of which the coupling with the phonon bath tends to destroy the quantum coherences $\sigma(0, 1, t)$ and $\sigma(1, 0, t)$. Note that $\Gamma = w$ when $V = 1$. In the same way, the parameter $\gamma = \gamma_{11} + \gamma_{00}^*$ accounts for a coupling between the two coherences mediated by the phonon bath. Therefore, by inserting Eq.(40) into Eq.(39), $\Delta W(z)$ is expressed as

$$\Delta W(z) = \frac{2\hat{\Phi}^2}{z + \Gamma + \gamma} \begin{pmatrix} 1 & -1 \\ -1 & 1 \end{pmatrix} \tag{41}$$

At this step, Eqs.(38) and (41) yield the required expression of the restricted Green operator so that the Laplace transform of the population difference is written as

$$\Delta\tilde{g}(z) = \frac{1}{z + 2\Gamma + \frac{4\hat{\Phi}^2}{z+\Gamma+\gamma}} \tag{42}$$

By performing the invert Laplace transform, $\Delta g(t)$ is finally expressed as

$$\Delta g(t) = e^{-rt}[\cos(\Omega t) - \frac{\Gamma - \gamma}{2\Omega}\sin(\Omega t)] \tag{43}$$

where $\Omega = \sqrt{4\hat{\Phi}^2 - (\Gamma - \gamma)^2/4}$ and $r = (3\Gamma + \gamma)/2$.

To interpret and understand the physics involved in Eq.(43), it is interesting to mention that this solution can be found directly by solving the quantum kinetic equation Eq.(22) in the special case $V = 1$. Indeed, this equation reduces to a system of four equations as

$$\begin{aligned}
\dot{q}(t) &= 0 \\
\dot{C}(t) &= -(\Gamma - \gamma)C(t) \\
\Delta\dot{g}(t) &= -2\hat{\Phi}J(t) - 2\Gamma\Delta g(t) \\
\dot{J}(t) &= 2\hat{\Phi}\Delta g(t) - (\Gamma + \gamma)J(t)
\end{aligned} \tag{44}$$

where $q(t) = \sigma(0,0,t) + \sigma(1,1,t)$ and $\sigma(0,1,t) = (C(t) + iJ(t))/2$

The first equation in Eq.(44) describes the conservation of the total number of quanta and it yields the vanishing eigenvalue in the spectrum of the effective Liouvillian. By contrast, the second equation characterizes how the phonon bath breaks the coherence between $\mid 0\rangle$ and $\mid 1\rangle$. It is a pure dephasing mechanism which is responsible for the occurrence of a purely imaginary eigenvalue $\lambda = -i(\Gamma - \gamma)$ in the spectrum of the effective Liouvillian. The last two equations, whose the solution is given by Eq.(43), describe the energy transfer between the states $\mid 0\rangle$ and $\mid 1\rangle$ which results from the competition between two processes. Indeed, the coherent part of the effective Liouvillian leads to a coupling between the populations and the coherences which favors the occurrence of oscillations. These oscillations, which the frequency is equal to $2\hat{\Phi}$, describe the delocalization of the polaron between the two sites of the dimer. However, the influence of the phonon bath is twofold. First, it allows for incoherent hops between the two sites of the dimer due to the stochastic fluctuations of the effective hopping constant. Then, it tends to destroy the coherence between the two sites and yields the damping of the imaginary part of the coherence.

As shown in Eq.(43) the competition between these two processes leads to the decay of the population difference which finally reaches a zero value describing a uniform distribution at equilibrium. In addition, its favors the occurrence of oscillations depending on the value of the parameter Ω. For real value of Ω, i.e. when $4\hat{\Phi}^2 \geq (\Gamma - \gamma)^2/4$, the population difference exhibits oscillations which the frequency is lower than the Bohr frequency $2\hat{\Phi}$ of the unperturbed dimer. By contrast, when $4\hat{\Phi}^2 < (\Gamma - \gamma)^2/4$, a purely exponential decay occurs. In fact,

$\Gamma - \gamma$ represents the difference between the incoherent transition rate and the dephasing constant connected to the damping of the coherence. Therefore, if the phonon bath leads to a fast incoherent energy transfer, or to a fast quantum decoherence, then the population difference does not have enough time to develop oscillations. This feature characterizes the fact that the population and the coherence cannot interact if either the population difference or the coherence disappear over a timescale shorter than $(2\hat{\Phi})^{-1}$.

However, in the situation studied here, the population difference exhibits oscillations with frequency Ω and damping rate r. Therefore, these oscillations produce two complementary eigenvalues $\lambda = \pm\Omega - ir$ in the spectrum of the effective Liouvillian, as observed in Fig. 4. To compare this theoretical calculations with our numerical results, let us mention that when $T = 100$ K, the relevant parameters are equal to $\Gamma = 0.445$ cm^{-1}, $\gamma = -0.375$ cm^{-1} and $\hat{\Phi} = 14.073$ cm^{-1}. Therefore, $\Omega = 14.068$ cm^{-1} and $r = 0.48$ cm^{-1}, in a perfect agreement with the results displayed in Figs. 2 and 4.

6.3 Approximated results for $V \geq 2$

In the general situation $V \geq 2$, $\mathcal{W}(z)$ cannot be calculated exactly so that several simplifying approximations are invoked. First, we apply the secular approximation in which the population-coherence coupling mediated by the relaxation operator is neglected, i.e. $P\mathcal{R}Q = 0$. Then, the interaction between the coherences mediated by the phonon bath is disregarded. The restriction of the relaxation operator to the coherences is thus assumed to be diagonal, i.e. $Q\mathcal{R}Q = g$, where g is the diagonal matrix which the elements $g_{pp'} = \mathcal{R}(pp', pp')$ describe each dephasing constant. They are defined as

$$\begin{aligned} g_{pp'} = &\Gamma_{p+1,p'}(p+1)(V-p) + \Gamma^*_{p'+1,p}(p'+1)(V-p') \\ &+ \Gamma_{p-1,p'}p(V-p+1) + \Gamma^*_{p'-1,p}p'(V-p'+1) \end{aligned} \tag{45}$$

Finally, the polaron Liouvillian $\mathcal{L}_{po} = \mathcal{L}_0 + \delta\mathcal{L}$ is expressed as the sum of its diagonal part $\mathcal{L}_0$ and its non diagonal part $\delta\mathcal{L}$. In the local basis $\mid p_1, p_2^\dagger\rangle\rangle$, $\mathcal{L}_0$ characterizes the Bohr frequencies $\epsilon_{p_1} - \epsilon_{p_2}$ whereas $\delta\mathcal{L}$ describes coherent hops. Therefore, within these approximations, $\Delta W(z)$ is expanded in a perturbative series as

$$\Delta W(z) = \sum_m P\delta\mathcal{L}Q\frac{1}{z+g+i\mathcal{L}_0}(-iQ\delta\mathcal{L}Q\frac{1}{z+g+i\mathcal{L}_0})^m Q\delta\mathcal{L}P \tag{46}$$

These different approximations can be used to evaluate the population difference. Nevertheless, a general calculation still remains difficult so that we

consider only the two asymptotic situations corresponding to the short time limit and to the long time limit, respectively.

6.3.1 Short time behavior

In the short time limit, the evolution of $\Delta g(t)$ corresponds to the behavior of $\Delta\tilde{g}(z)$ when $z \to \infty$. Consequently, only the lowest order of the perturbative expansion of $\Delta W(z)$ (Eq.(46)) will contribute significantly. This contribution, denoted $\Delta W^{(2)}(z)$ (see Fig. 10), is described in details in Appendix A. It characterizes the transitions between the states $\mid p\rangle$ and $\mid p \pm 1\rangle$ which result from the occurrence of a quantum state involving the coherent superimposition of these states. In other words, it refers to the indirect coupling between the populations $\mid p, p^{\dagger}\rangle\rangle$ and $\mid (p \pm 1), (p \pm 1)^{\dagger}\rangle\rangle$ mediated by the coherences $\mid (p \pm 1), p^{\dagger}\rangle\rangle$ and $\mid p, (p \pm 1)^{\dagger}\rangle\rangle$.

Therefore, by expressing the incoherent rate matrix $W = W_0 + \delta W$ (Eq.(32)) as the sum of its diagonal part W_0 and its non diagonal part δW, the perturbative expansion of $\mathcal{W}(z)$ with respect to δW is performed. At the lowest order, it is written as

$$\mathcal{W}(z) \approx \mathcal{P}(W + \Delta W^{(2)}(z))\mathcal{P} - \mathcal{P}\delta W\mathcal{Q}\frac{1}{z + W_0}\mathcal{Q}\delta W\mathcal{P} \tag{47}$$

After some straightforward algebraic manipulations, the required elements of the effective transition rate matrix are defined as

$$\begin{aligned}
\mathcal{W}_{00}(z) &= W_{0\to1} + \frac{2(z + g_{01})V\hat{\Phi}^2}{(z + g_{01})^2 + (\epsilon_1 - \epsilon_0)^2} - \frac{W_{0\to1}W_{1\to0}}{z + W_{1\to0} + W_{1\to2}} \\
\mathcal{W}_{0V}(z) &= -\frac{W_{0\to1}W_{1\to0}}{z + W_{1\to0} + W_{1\to2}}\delta_{V2}
\end{aligned} \tag{48}$$

Therefore, by inserting Eq.(48) into Eq.(37), and by taking advantage of the fact that $\hat{\Phi}$ is larger than the different elements of the relaxation operator, the Laplace transform of the population difference is written as

$$\Delta\tilde{g}(z) \approx \frac{V}{z + W_{0\to1}}[1 - \frac{2V\hat{\Phi}^2}{(z + g_{01})^2 + (\epsilon_1 - \epsilon_0)^2}] \tag{49}$$

By performing the invert Laplace transform, the time evolution of the population difference is finally expressed as

$$\Delta g(t) \approx Ve^{-W_{0\to1}t}[1 - \frac{2V\hat{\Phi}^2}{r^2 + \omega^2}(1 - e^{-rt}\cos(\omega t) - \frac{r}{\omega}e^{-rt}\sin(\omega t))] \tag{50}$$

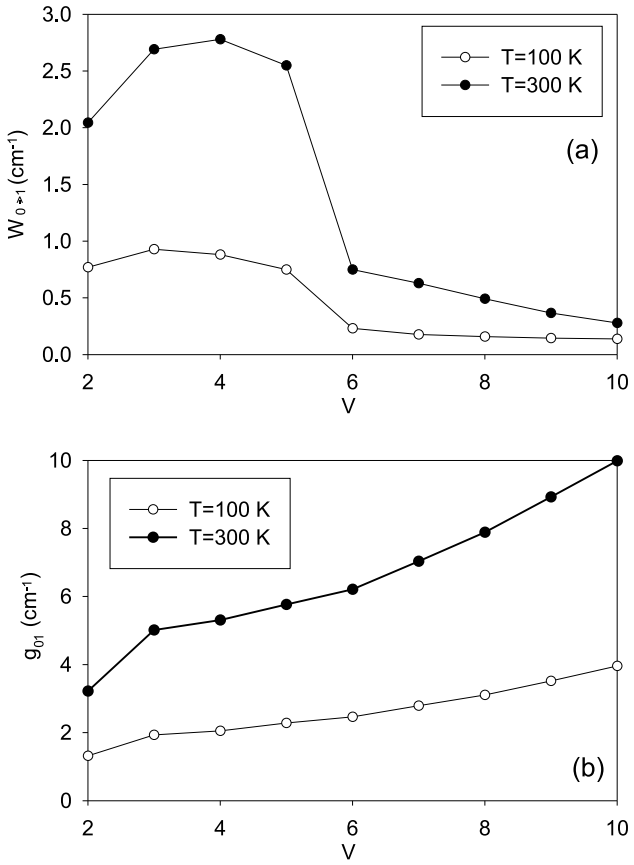

Fig. 11. (a) Incoherent transition rate $W_{0\to 1}$ and (b) dephasing constant g_{01} vs the number of quanta V for T=100 K (open circles) and T=300 K (full circle). The parameters are $\Phi = 7.8$ cm^{-1}, $A = 8$ cm^{-1}, $E_B = 3$ cm^{-1} and $\Omega_c = 92$ cm^{-1}

where $\omega = \epsilon_1 - \epsilon_0$ and $r = g_{01} - W_{0\to 1}$. Note that due to the reflection symmetry, the relations $W_{0\to 1} = W_{V\to V-1}$, $g_{01} = g_{VV-1}$ and $\omega = \epsilon_{V-1} - \epsilon_V$ are verified. In a perfect agreement with the numerical results, Eq.(50) clearly shows that in the short time limit the population difference exhibits a zero frequency component which decreases exponentially according to the decay rate $W_{V\to V-1}$. This component supports a damped high-frequency modulation which the frequency and the damping rate are equal to $\omega = \epsilon_{V-1} - \epsilon_V$ and g_{VV-1}, respectively.

To interpret this behavior, let us remain that in the short time limit $\Delta g(t)$ is proportional to the population of the state $\mid V\rangle$ which is initially excited. Therefore, the origin of the time evolution is twofold. First, the energy transfer between the dimer and the phonon bath yields an incoherent transition from $\mid V\rangle$ to $\mid V-1\rangle$. As a result, the population of the state $\mid V\rangle$ decreases according to the decay rate $W_{V\to V-1}$. Then, the Hamiltonian of the unperturbed dimer leads to a coupling $\sqrt{V}\hat{\Phi}$ between the states $\mid V\rangle$ and $\mid V-1\rangle$ so that the dimer develops a coherent superimposition of these states. Consequently, the population of $\mid V\rangle$ exhibits a modulation which oscillates according to a frequency given by the energy difference $\epsilon_{V-1} - \epsilon_V$. However, the coupling with the phonon bath tends to break the coherence of this superimposition and it favors a decay of the oscillations governed by the dephasing constant g_{VV-1}.

These calculations allow for a complete interpretation of the numerical results displayed in Fig. 2, 3, 6 and 8. Indeed, the energy difference $\epsilon_{V-1} - \epsilon_V$, equal $(V-1)(2A+E_B)$, increases with both the number of quanta V and the anharmonicities A and E_B. As illustrated in Fig. 11, the dephasing constant g_{VV-1} increases with the number of quanta and with the temperature. Finally, as shown in Eq.(50), the amplitude of the modulation typically scales as $2(V\hat{\Phi}/(V-1)(2A+E_B))^2$. It varies slowly with the number of quanta and it decreases with the anharmonicities. It also decreases with the temperature which reduces the effective hopping constant due to the dressing effect.

Finally, let us discuss the occurrence of a transition between the two dynamical regimes in terms of the behavior of the incoherent transition rate $W_{0\to 1} = W_{V\to V-1}$. As shown in Fig. 11, above a critical value V^* the decay rate becomes suddenly very small. This behavior originates in its dependence on the energy difference between the states $\mid V\rangle$ and $\mid V-1\rangle$. Indeed, as detailed in the Appendix B, the main contribution of the rate decreases with the energy difference to finally vanishes when $\epsilon_{V-1} - \epsilon_V$ becomes greater than the phonon cutoff frequency, i.e. $(V-1)(2A+E_B) > \Omega_c$. This behavior results form the energy exchange between the dimer and the phonon bath mediated by single phonon processes. However, transitions induced by multi-phonon exchanges remain but their contribution to the decay rate is rather small. Consequently, a transition takes place for a critical value of the number of quanta $V^* = 1 + \Omega_c/(2A+E_B)$. For $A = 8$ cm^{-1}, $E_B = 3$ cm^{-1} and $\Omega_c = 92$ cm^{-1}, this critical value is equal to $V^* = 5.84$, in a perfect agreement with the observations made in Fig. 2 and 3. In the same way, we can define a critical value for the anharmonicity A which, for $V = 5$, $E_B = 3$ cm^{-1} and $\Omega_c = 92$ cm^{-1}, is equal to $A^* = 10$ cm^{-1}, as observed in Fig. 8. Therefore, when $V < V^*$ (or $A < A^*$), the population difference shows an exponential decay due to the rather strong value of the transition rate $W_{V\to V-1}$. By contrast, when $V > V^*$ (or $A > A^*$), the transition rate becomes negligible so that the population difference supports a small amplitude modulation but without any exponential decay. This latter regime is the quantum counterpart of the classical self-trapping which only occurs over a timescale of about a few picoseconds.

6.3.2 Long time behavior

In the long time limit, the evolution of the population difference is described by the behavior of $\Delta\tilde{g}(z)$ when $z \to 0$. As shown in Eq.(46), the perturbative expansion of $\Delta W(z)$ defines pathways in the Liouville space which connect two populations. Therefore, for a specific pathway, a matrix element $\Delta W_{pp'}(z)$ is expressed in terms of the product of the free propagators $(z + g_{p_1p_2} + i(\epsilon_{p_1} - \epsilon_{p_2}))^{-1}$ associated to the coherences $\mid p_1, p_2^\dagger\rangle\rangle$ lying along the pathway. The Liouville space contains two kinds of coherences. First, it supports a set of coherences $\mid p_1, p_2^\dagger\rangle\rangle$ which the free evolution is governed by a non vanishing

frequency $\epsilon_{p_1} - \epsilon_{p_2}$. Then, due to the reflection symmetry, the Liouville space exhibits a set of $(V+1)$ coherences which the characteristic frequencies vanish. These coherences, which satisfy the relation $p_1+p_2 = V$, are resonant with the populations and thus they play a key role in the long time limit. Therefore, to evaluate $\Delta W(z)$, the propagators $(z + g_{p_1p_2} + i(\epsilon_{p_1} - \epsilon_{p_2}))^{-1}$ for which $\epsilon_{p_1} \neq \epsilon_{p_2}$ can be approximated by their value for $z = 0$. Then, among the propagators $(z+g_{p_1p_2})^{-1}$ involving resonant coherences, the main contributions in the long time limit will involve those with the smallest dephasing constant. Our numerical study has revealed that only the two coherences $\mid V, 0^\dagger\rangle\rangle$ and $\mid 0, V^\dagger\rangle\rangle$ satisfy this requirement (see Fig. 10).

As a consequence, when $z \to 0$, $\Delta W(z)$ is approximated as

$$\Delta W(z) \approx \Delta W^{(NR)}(0) + w^{(R)}(z) \tag{51}$$

where $w^{(R)}(z)$ is the resonant contribution which describes a population-population interaction mediated by the coherences $\mid V, 0^\dagger\rangle\rangle$ and $\mid 0, V^\dagger\rangle\rangle$, whereas $\Delta W^{(NR)}(0)$ characterizes all the other contributions. At the pth order, $\Delta W^{(NR)}(0)$ is proportional to the ratio $\hat{\Phi}^p/\Delta\epsilon^{p-1}$, where $\Delta\epsilon$ is the typical energy difference between two basis vectors. For realistic systems in which the anharmonicities are greater than the effective hopping constant, it represents a rather small correction and only the second order will contribute significantly, i.e. $\Delta W^{(NR)}(0) \approx \Delta W^{(2)}(0)$. By contrast, at the lowest order equal to 2V, the resonant contribution $w^{(R)}(z)$ characterizes a coupling between the two populations $\mid V, V^\dagger\rangle\rangle$ and $\mid 0, 0^\dagger\rangle\rangle$ mediated by the coherences $\mid V, 0^\dagger\rangle\rangle$ and $\mid 0, V^\dagger\rangle\rangle$. Therefore, as detailed in Appendix C, the corresponding matrix elements are defined as

$$w_{00}^{(R)}(z) = \frac{\Delta E}{2(z + g_{00})} \tag{52}$$

where ΔE (Eq.(14)) is the energy splitting between the two lowest energy levels of the dimer and where $w_{0V}^{(R)}(z) = -w_{00}^{(R)}(z)$.

In that context, the effective transition rate matrix $\mathcal{W}(z)$ is expressed as

$$\mathcal{W}(z) = \mathcal{P}w^{(R)}(z)\mathcal{P} + \mathcal{P}\bar{W}\mathcal{P} - \mathcal{P}\bar{W}\mathcal{Q}[z + \bar{W}]^{-1}\mathcal{Q}\bar{W}\mathcal{P} \tag{53}$$

where $\bar{W} = W+\Delta W^{(2)}(0)$ characterizes the transitions between nearest neighbor populations due to both a direct coupling with the phonon bath and an interaction mediated by the non resonant coherences. Note that since the resonant term $w^{(R)}(z)$ is a $2V$th order contribution, it has been neglected to describe the coupling between the populations $\mid 0, 0^\dagger\rangle\rangle$ and $\mid V, V^\dagger\rangle\rangle$ via by the other populations.

At this step, by expressing $\bar{W} = \bar{W}_0 + \delta\bar{W}$ in terms of its diagonal $\bar{W}_0$ and non diagonal part $\delta\bar{W}$, the perturbative expansion of the effective transition rate matrix $\mathcal{W}(z)$ with respect to $\delta\bar{W}$ is performed. This procedure, detailed in Appendix D, yields the two required elements $\mathcal{W}_{00}(z)$ and $\mathcal{W}_{0V}(z)$ to finally obtain the Laplace transform of the population difference as

$$\Delta\tilde{g}(z) = \frac{V}{z + \bar{W}_{eff} + \frac{\Delta E}{z+g_{00}}} \tag{54}$$

where, at the lowest order, $\bar{W}_{eff}$ is defined as

$$\bar{W}_{eff} = \bar{W}_{00} - \frac{\bar{W}_{01}\bar{W}_{10}}{\bar{W}_{11}}(1 - \delta_{V2}) \tag{55}$$

In a general way, $\bar{W}_{eff}$ (see Appendix D) is the effective rate for the incoherent transition between the states $\mid 0\rangle$ and $\mid V\rangle$. Such a transition results from a series of hops between nearest neighbor basis vectors according to the global rate matrix $\bar{W}$. Therefore, its incoherent nature must be understood in the sense that it does not involve any coupling with the resonant coherences $\mid V, 0^\dagger\rangle\rangle$ and $\mid 0, V^\dagger\rangle\rangle$.

By performing the invert Laplace transform of Eq.(54), the time evolution of the population difference is finally expressed as

$$\Delta g(t) = e^{-rt}[\cos(\Omega t) - \frac{\bar{W}_{eff} - g_{00}}{2\Omega}\sin(\Omega t)] \tag{56}$$

where $\Omega = \sqrt{\Delta E^2 - (\bar{W}_{eff} - g_{00})^2/4}$ and $r = (\bar{W}_{eff} + g_{00})/2$.

As shown in Eq.(56), the long time behavior of the population difference results from the competition between two main mechanisms. The first mechanism originates in the coherent part of the effective Liouvillian. It yields a coupling between the populations $\mid V, V^\dagger\rangle\rangle$ and $\mid 0, 0^\dagger\rangle\rangle$ through their interaction with the resonant coherences $\mid V, 0^\dagger\rangle\rangle$ and $\mid 0, V^\dagger\rangle\rangle$. This coupling corresponds to the superimposition of the states $\mid V\rangle$ and $\mid 0\rangle$ which yields the delocalization of a V-polaron bound state. This delocalization leads to a coherent energy transfer responsible for the oscillations of the population difference at a frequency ΔE equal to the energy splitting between the two lowest energy levels of the dimer. The origin of the second mechanism, which prevents the coherent energy transfer, is twofold. First, the phonon bath favors the quantum decoherence of the superimposition involving $\mid V\rangle$ and $\mid 0\rangle$. It is a pure dephasing effect which yields the decay of the corresponding coherence according to the dephasing constant $g_{00} = g_{0V}$. Note that g_{00} is equal to the incoherent rate $W_{0\to 1}$ (see Eqs.(33) and (45)). Then, a series of transitions between nearest

neighbor basis vectors takes place. It yields a redistribution of the population of the basis vectors and it ensures the convergence of the population difference to a vanishing value at equilibrium. This series of transitions is described by the effective rate $\bar{W}_{eff}$ and it involves both purely incoherent hops due to the coupling with the phonon bath and population exchanges mediated by the interaction with non resonant coherences.

As shown in Eq.(56), the competition between these two mechanisms leads to the occurrence of two dynamical regimes depending on the ratio between the energy splitting ΔE and the parameter $\mid \bar{W}_{eff} - g_{00} \mid /2$. When this ratio is greater than unity, the population difference exhibits damped oscillations describing a limited coherent energy transfer. The frequency of these oscillations is slightly red shifted form the value of the energy splitting ΔE and the decay rate is given by $r = (\bar{W}_{eff} + g_{00})/2$. By contrast, when the ratio is smaller than unity, $\Delta g(t)$ shows a purely exponential decay which the rate, in the long time limit, is expressed as $r' = (\bar{W}_{eff} + g_{00})/2 + \sqrt{(\bar{W}_{eff} - g_{00})^2/4 - \Delta E^2}$.

These theoretical results give a complete understanding of the numerical features presented in Section 5. Indeed, when $\Phi = 7.8\ \mathrm{cm}^{-1}$, $A = 8\ \mathrm{cm}^{-1}$, $E_B = 3\ \mathrm{cm}^{-1}$, $\Omega_c = 92\ \mathrm{cm}^{-1}$, $T = 100K$, the evaluation of the ratio $2\Delta E/ \mid \bar{W}_{eff} - g_{00} \mid$ shows that the transition between the two dynamical regimes takes place when the number of quanta ranges between $V^* = 5$ and $V^* = 6$, in a perfect agreement with the results displayed in Fig. 2. When $V < V^*$, the detailed study of the effective rate W_{eff} in Appendix D reveals that the long time decay rate r is typically of about the incoherent rate $W_{0\to 1}$. As a result, $W_{eff} \approx g_{0V} << \Delta E$ so that both the depopulation of the states $\mid 0\rangle$ and $\mid V\rangle$ and the dephasing of the coherence between these two states occur over a same timescale larger than ΔE^{-1}. Population and coherence couple to each other and they produce oscillations of the population difference whose frequency is about the energy splitting ΔE (Eq.(14)). This frequency decreases with both the number of quanta, the anharmonicities and the temperature, as observed in Fig. 2,3,4 and 8. In this regime, the return to the equilibrium is thus ensured by a series of population exchanges due to the energy transfer with the phonon bath. When $V > V^*$, g_{00} is negligible. Since ΔE is very small, the depopulation of the states $\mid 0\rangle$ and $\mid V\rangle$ is faster than the dephasing of the coherence between these two states and it occurs over a timescale shorter than ΔE^{-1}. As a consequence, a purely exponential decay takes place according to a decay rate r' typically of about W_{eff}. From Appendix D, W_{eff} is approximately given by $\Delta W_{01}^{(2)}(0)\Delta W_{12}^{(2)}(0)/\Delta W_{11}^{(2)}(0)$ so that the return to the equilibrium is governed by a series of population exchanges mediated by the coupling with the non resonant coherences. Note that, as illustrated in Figs. 7 and 9, the theoretical expression of the decay rate in the long time limit, either equal to r or r' depending on the dynamical regimes, clearly reproduces the behavior of the exact rate obtained from the diagonalization of the effective Liouvillian.

To conclude, let us mention that the transition in the long time limit discriminates between two mechanisms for the return to the equilibrium. It originates in the disappearance of an efficient energy transfer between the dimer and the phonon bath. Since only single phonon exchanges contribute significantly to this transfer, the transition occurs when the energy required to leave the initial state $\mid V\rangle$ is greater than the phonon cutoff frequency, i.e. $\epsilon_{V-1} - \epsilon_V > \Omega_c$. In other words, the transitions in both the long time and the short time limit have the same origin.

A Expression of the transition rate matrix $\Delta W^{(2)}(z)$

From Eq.(46), the second order expansion of the operator $\Delta W(z)$ is defined as

$$\Delta W^{(2)}(z) = P\mathcal{L}_{po}Q\frac{1}{z+g+i\mathcal{L}_0}Q\mathcal{L}_{po}P \tag{A.1}$$

Therefore, by inserting into Eq.(A1) the local basis set which generates the Liouville space, the matrix element of $\Delta W^{(2)}(z)$ are expressed as

$$\Delta W^{(2)}_{pp'}(z) = \sum_{p_1,p_2} \frac{\langle\langle p^\dagger, p \mid \mathcal{L}_{po} \mid p_1, p_2^\dagger\rangle\rangle\langle\langle p_1^\dagger, p_2 \mid \mathcal{L}_{po} \mid p', p'^\dagger\rangle}{z + g_{p_1p_2} + i(\epsilon_{p_1} - \epsilon_{p_2})} \tag{A.2}$$

Since the polaron Liouvillian connects nearest neighbor basis vectors in the Liouville space, the non vanishing elements satisfy $p' = p$ and $p' = p \pm 1$. They are defined as

$$\begin{aligned}
\Delta W^{(2)}_{pp+1}(z) &= -\frac{2(z+g_{pp+1})(p+1)(V-p)\hat{\Phi}^2}{(z+g_{pp+1})^2 + (\epsilon_p - \epsilon_{p+1})^2} \\
\Delta W^{(2)}_{pp-1}(z) &= -\frac{2(z+g_{pp-1})p(V-p+1)\hat{\Phi}^2}{(z+g_{pp-1})^2 + (\epsilon_p - \epsilon_{p-1})^2}
\end{aligned} \tag{A.3}$$

where $\Delta W^{(2)}_{pp}(z) = -\Delta W^{(2)}_{pp-1}(z) - \Delta W^{(2)}_{pp+1}(z)$.

B Expression of the transition rate $W_{p\to p'}$

From Eq.(33), the incoherent transition rate $W_{p\to p'}$ is expressed in terms of the parameter $\Gamma_{p'p}$ defined in Eq.(24). This parameter involves the correlation function of the fluctuations of the polaron-phonon coupling (Eq.(11)) and the

free propagators of the unperturbed dimer. In that context, since the small polaron binding energy is about one order of magnitude smaller than the phonon cutoff frequency, the dressing operators can be linearized. Therefore, the fluctuations V_{01} of the polaron hopping constant is approximately written as

$$V_{01} \approx \sum_q \frac{4\Phi\Delta_0}{\sqrt{N}\Omega_c} \cos(q/2)\sqrt{\mid \sin(q/2) \mid}(e^{-iq/2}a_q^\dagger - e^{iq/2}a_q) \tag{B.1}$$

where $V_{10} = -V_{01}$. In addition, for a sufficiently strong anharmonicity, the free propagator of the unperturbed dimer reduces to the evolution operator obtained in the limit $\Phi = 0$, i.e. $G_{po}(p,p,t) \approx \exp(-i\epsilon_p t)$. In this context, Eq.(24) can be calculated straightforwardly as

$$\Gamma_{p'p} = \frac{16\Phi^2 E_B}{\Omega_c^3} \mid \Delta\epsilon \mid \sqrt{1-(\frac{\Delta\epsilon}{\Omega_c})^2} \begin{cases} n_B(\mid \Delta\epsilon \mid) & \text{if } \Delta\epsilon < 0 \\ 1 + n_B(\mid \Delta\epsilon \mid) & \text{if } \Delta\epsilon > 0 \end{cases} \tag{B.2}$$

where $\Delta\epsilon = \epsilon_p - \epsilon'_p$ and where n_B denotes the Bose-Einstein distribution.

In other words, when $\epsilon_p < \epsilon'_p$, the incoherent transition from $\mid p\rangle$ to $\mid p'\rangle$ results from the absorption of a single phonon. By contrast, when $\epsilon_p > \epsilon'_p$, the transition occurs due to the emission of a single phonon. In fact, because of the linearization of the dressing operators, Eq.(B2) describes single phonon processes, only, for which the corresponding rates vanish when the exchanged energy exceeds the phonon cutoff frequency. In that case, multi-phonon exchanges remain but their contributions to the rates are very small.

C Expression of the transition rate matrix $w^{(R)}(z)$

As mentioned in the text, the lowest order of the operator $w^{(R)}(z)$ describes the coupling between the populations $\mid 0, 0^\dagger\rangle\rangle$ and $\mid V, V^\dagger\rangle\rangle$ mediated by the resonant coherences $\mid 0, V^\dagger\rangle\rangle$ and $\mid V, 0^\dagger\rangle\rangle$. It corresponds to the $2V$th order expansion of $\Delta W(z)$ (see Eq.(46)) and its matrix elements are defined as

$$\begin{aligned} W_{0V}^{(R)}(z) = (-1)^{V-1} & \frac{\langle\langle 0^\dagger, 0 \mid \delta\mathcal{L} \mid 1, 0^\dagger\rangle\rangle ... \langle\langle (V-1)^\dagger, 0 \mid \delta\mathcal{L} \mid V, 0^\dagger\rangle}{(z + g_{10} + i(\epsilon_1 - \epsilon_0))...(z + g_{V-10} + i(\epsilon_{V-1} - \epsilon_0))} \\ \times \frac{1}{z + g_{V0}} & \times \frac{\langle\langle V^\dagger, 0 \mid \delta\mathcal{L} \mid V, 1^\dagger\rangle\rangle ... \langle\langle V^\dagger, V-1 \mid \delta\mathcal{L} \mid V, V^\dagger\rangle}{(z + g_{V1} + i(\epsilon_V - \epsilon_1))...(z + g_{VV-1} + i(\epsilon_V - \epsilon_{V-1}))} \\ + c.c. & \end{aligned} \tag{C.1}$$

where $W_{00}^{(R)}(z) = -W_{0V}^{(R)}(z)$. The first term in the right-hand-side of Eq.(C1) characterizes the Liouville pathway containing the coherence $\mid V, 0^{\dagger}\rangle\rangle$. The symbol c.c. represents the complex conjugate which refers to the pathway involving the coherence $\mid 0, V^{\dagger}\rangle\rangle$. After some straightforward manipulations and by taking advantage of the reflection symmetry, Eq.(C1) is finally rewritten as

$$w_{0V}^{(R)}(z) = -\frac{2V!^2\hat{\Phi}^{2V}}{z+g_{00}} \prod_{p=1}^{V-1} \frac{1}{(z+g_{p0})^2 + (\epsilon_p - \epsilon_0)^2} \tag{C.2}$$

Since the energy difference between the basis vectors are greater than the dephasing constant of about several orders of magnitude, the $z + g_{po}$ dependence in the product of Eq.(C2) can be neglected so that

$$\prod_{p=1}^{V-1} (\epsilon_p - \epsilon_0)^2 = (V-1)!^4 (2A + E_B)^{2(V-1)} \tag{C.3}$$

By inserting Eq.(C3) into Eq. (C2), we finally obtain

$$w_{0V}^{(R)}(z) = -2(\frac{V\hat{\Phi}^V}{(V-1)!(2A+E_B)^{V-1}})^2 \frac{1}{z+g_{00}} \tag{C.4}$$

which is equivalent to Eq.(52).

D Expression of the effective transition rate $\bar{W}_{eff}$

According to Eq.(53), the perturbative expansion of the effective transition rate matrix $\mathcal{W}(z)$ with respect to the non diagonal part $\delta\bar{W}$ of the global incoherent rate $\bar{W} = \bar{W}_0 + \delta\bar{W}$ is written as

$$\begin{aligned} \mathcal{W}(z) &= \mathcal{P}w^{(R)}(z)\mathcal{P} + \mathcal{P}\bar{W}\mathcal{P} - \mathcal{P}\delta\bar{W}\mathcal{Q}\frac{1}{z+\bar{W}_0}\mathcal{Q}\delta\bar{W}\mathcal{P} \\ &+ \mathcal{P}\delta\bar{W}\mathcal{Q}\frac{1}{z+\bar{W}_0}\mathcal{Q}\delta\bar{W}\mathcal{Q}\frac{1}{z+\bar{W}_0}\mathcal{Q}\delta\bar{W}\mathcal{P} + ... \end{aligned} \tag{D.1}$$

The corresponding matrix elements are defined as

$$\begin{aligned} \mathcal{W}_{00}(z) &= w_{00}^{(R)} + \bar{W}_{00} - \frac{\bar{W}_{01}\bar{W}_{10}}{\bar{W}_{11}} - \frac{\bar{W}_{01}\bar{W}_{12}\bar{W}_{21}\bar{W}_{10}}{\bar{W}_{11}\bar{W}_{22}\bar{W}_{11}}(1-\delta_{V2}) + ... \\ \mathcal{W}_{0V}(z) &= w_{0V}^{(R)} - \frac{\bar{W}_{01}\bar{W}_{12}}{\bar{W}_{11}}\delta_{V2} + \frac{\bar{W}_{01}\bar{W}_{12}\bar{W}_{23}}{\bar{W}_{11}\bar{W}_{22}}\delta_{V3} + ... \end{aligned} \tag{D.2}$$

Therefore, at the lowest order, the difference $\mathcal{W}_{00}(z) - \mathcal{W}_{0V}(z)$ involved in the calculation of the population difference is expressed as

$$\mathcal{W}_{00}(z) - \mathcal{W}_{0V} = 2w_{00}^{(R)} + \bar{W}_{00} + \bar{W}_{eff} \tag{D.3}$$

where the effective incoherent rate $\bar{W}_{eff}$ is defined as

$$\bar{W}_{eff} = \bar{W}_{00} - \frac{\bar{W}_{01}\bar{W}_{10}}{\bar{W}_{11}}(1 - \delta_{V2}) \tag{D.4}$$

From the expression of the rates W for the purely incoherent transitions, and by using the results displayed in Appendix A, the different parameters used in Eq.(D4) are defined as

$$\begin{aligned}
\bar{W}_{00} &= 2VRe\Gamma_{10} + \frac{2V\hat{\Phi}^2 g_{01}}{((V-1)(2A+E_B))^2} \\
\bar{W}_{01} &= -2VRe\Gamma_{01} - \frac{2V\hat{\Phi}^2 g_{01}}{((V-1)(2A+E_B))^2} \\
\bar{W}_{10} &= -2VRe\Gamma_{10} - \frac{2V\hat{\Phi}^2 g_{01}}{((V-1)(2A+E_B))^2} \\
\bar{W}_{11} &= 2VRe\Gamma_{01} + 4(V-1)Re\Gamma_{21} + \frac{2V\hat{\Phi}^2 g_{01}}{((V-1)(2A+E_B))^2} \\
&\quad + \frac{4(V-1)\hat{\Phi}^2 g_{21}}{((V-3)(2A+E_B))^2}(1-\delta_{V3}) + \frac{4(V-1)\hat{\Phi}^2}{g_{21}}\delta_{V3}
\end{aligned} \tag{D.5}$$

References

[1] A. S. Davydov, N. I. Kisluka, Phys. Status Solidi 59 (1973) 465; Zh. Eksp. Teor. Fiz 71 (1976) 1090 [Sov. Phys. JETP 44 (1976) 571].

[2] A.C. Scott, Phys. Rep. 217 (1992)1 .

[3] P. L. Christiansen, A. C. Scott , *Davydov's Soliton Revisited*,(Plenum, New York, 1990).

[4] S. Aubry, Physica D103 (1997) 201.

[5] S. Flach, C.R. Willis, Phys. Rep. 295 (1998) 181.

[6] R.S. MacKay, Physica A 288 (2000) 174.

[7] A. J. Sievers, S. Takeno, Phys. Rev. Lett. 61 (1988) 970.

[8] D.W. Brown, Z. Ivic, Phys. Rev. B40 (1989) 9876.

[9] D.W. Brown, K. Lindenberg, X. Wang in: P. L. Christiansen, A. C. Scott (Eds.), Davydov's Soliton Revisited, Plenum, New York, 1990 .

[10] Z. Ivic, D. Kapor, M. Skrinjar, Z. Popovic, Phys. Rev. B 48 (1993) 3721.

[11] Z. Ivic, D. Kostic, Z. Przulj, D. Kapor, J. Phys. Condens. Matter 9 (1997) 413.

[12] J. Tekic, Z. Ivic, S. Zekovic, Z. Przulj, Phys. Rev. E 60 (1999) 821.

[13] V. Pouthier, Phys. Rev. E 68 (2003) 021909.

[14] V. Pouthier, C. Falvo, Phys. Rev. E 69 (2004) 041906.

[15] V. Pouthier, Phys. Rev. E 72 (2005) 031901.

[16] C. Falvo, V. Pouthier, J. Chem. Phys. 123 (2005) 184709.

[17] C. Falvo, V. Pouthier, J. Chem. Phys. 123 (2005) 184710.

[18] V. Fleuro, Chaos 13 (2003) 676.

[19] J.C. Eilbeck, Some exact results for quantum lattice problems in: L. Vasquez, R.S. Mackay, M. P. Zorzano (Eds), Proceedings of the Third Conference Localization and Energy Transfert in Nonlinear Systems, World Scientific, Singapore, 2003.

[20] J. C. Kimball, C. Y. Fong, Y. R. Shen, Phys. Rev. B 23 (1981) 4946.

[21] F. Bogani, G. Cardini, V. Schettino, P. L. Tasselli , Phys. Rev. B 42 (1990) 2307 .

[22] A. C. Scott, J. C. Eilbeck, H. Gilhoj, Physica D 78 (1994) 194.

[23] L. Proville, Phys. Rev. B 71 (2005) 1043306.

[24] V. Pouthier, C. Girardet, Phys. Rev. B 65 (2002) 035414.

[25] V. Pouthier, J. Chem. Phys. 118 (2003) 3736.

[26] V. Pouthier, J. Chem. Phys. 118 (2003) 9364 .

[27] V. Pouthier, Phys. Rev. B71 (2005) 115401.

[28] V. Pouthier, Physica D 213 (2006) 1.

[29] J. Edler, R. Pfister, V. Pouthier, C. Falvo, P. Hamm, Phys. Rev. Lett. 93 (2004) 106405.

[30] J.C. Eilbeck, P.S. Lomdahl and A.C. Scott, Physica D16 (1985) 318.

[31] V.M. Kenkre, D.K. Campbell, Phys. Rev. B 34 (1986) 4959.

[32] V. Szocs, P. Banacky, Phys. Rev. A 45 (1992) 5415.

[33] V. Szocs, P. Banacky, A. Zajac, Phys. Rev. A 45 (1990) 737.

[34] V. Szocs, P. Banacky, P. Reineker, Chem. Phys. 199 (1995) 1.

[35] B. Esser, D. Hennig, Z. Phys. B 83 (1991) 285.

[36] B. Esser, D. Hennig, Philos. Mag. B 65 (1992) 887.

[37] D. Hennig, Phys. Scr. 46 (1992) 14.

[38] D. Hennig, J. Phys. A 25 (1992) 285.

[39] D. Hennig, B. Esser, Phys. Rev. A 46 (1992) 4569.

[40] V. M. Kenkre, G. P. Tsironis, Phys. Rev. B 35 (1987) 1473.

[41] V. M. Kenkre, H.-L. Wu, Phys. Lett. A 135 (1989) 120.

[42] V. M. Kenkre, H.-L. Wu, Phys. Rev. B 39 (1989) 6907.

[43] P. Grigolini, H.-L. Wu, V. M. Kenkre, Phys. Rev. B 40 (1989) 7045.

[44] G. P. Tsironis, V. M. Kenkre, Phys. Lett. A 127 (1989) 209.

[45] G. P. Tsironis, V. M. Kenkre, and D. Finley, Phys. Rev. A 37 (1988) 4474.

[46] L. Bernstein, J.C. Eilbeck and A.C. Scott, Nonlinearity 3 (1990) 293.

[47] E. Wright, J.C Eilbeck, M.H. Hays, P.D. Miller and A.C. Scott, Physica D 69 (1993) 18.

[48] G. Kalosakas and A.R. Bishop, Phys. Rev. A 65 (2002) 043616.

[49] G. Kalosakas, A.R. Bishop, and V.M. Kenkre, Phys. Rev. A 68 (2003) 023602.

[50] G. Kalosakas, A.R. Bishop, and V.M. Kenkre, J. Phys. B:At. Mol. Opt. Phys. 36 (2003) 3233.

[51] I. G. Lang, Yu. A. Firsov, Sov. Phys. JETP 16 (1962) 1293.

[52] S. Mukamel, *Principles of Nonlinear Optical Spectroscopy*, (Oxford University Press, Oxford, 1995).

[53] R. Zwanzig, Lect. Theoret. Phys. 3 (1961) 106; Physica 30 (1964) 1109;J. Chem. Phys. 33 (1960) 1338.

[54] H. Mori Prog. Theoret. Phys. 33 (1965) 423; Prog. Theoret. Phys. 34 (1965) 399.